CONTROL OF BUCKLE FOLDING AND THE LOCAL STRESS FIELD ON THE DISTRIBUTION OF WIDESPREAD BRECCIATION IN THE CLONCURRY DISTRICT, MT ISA BLOCK, AUSTRALIA

CONTROL OF BUCKLE FOLDING AND THE LOCAL STRESS FIELD ON THE DISTRIBUTION OF WIDESPREAD BRECCIATION IN THE CLONCURRY DISTRICT, MT ISA BLOCK, AUSTRALIA

4.1 INTRODUCTION

Tectonic and magmatic-hydrothermal brecciation can be thought of as distinct processes (e.g. Sillitoe, 1985), with fracturing being facilitated in the former predominantly by high strain rate and/or low mean stress, and in the latter predominantly by high fluid pressure. However, each of the above variables is important in facilitating fracturing and brecciation. In many cases, for instance within some fault zones, tectonic and magmatic-hydrothermal breccia styles become difficult to distinguish (e.g. Sibson, 1977; Sillitoe, 1985). As such, it is perhaps more appropriate to consider brecciation reflecting mechanical (i.e. high strain rate and low mean stress) and hydraulic parameters (i.e. high fluid pressure) as end member processes. In regions undergoing synchronous deformation and magmatism, brecciation will in most cases be facilitated to varying degrees by elevated pore fluid pressure, and at the same time will inherently exploit zones that are more conducive to fracturing, either because of pre-existing weaknesses, or locally high strain rate, high differential stress or low mean stress. These zones of brecciation need not be limited to fault zones, as in a heterogeneous crust significant local variations can exist in the regional stress field.

Throughout the Eastern Succession, large areas of Mary Kathleen Group stratigraphy are brecciated, and formally recognized as the Corella, Gilded Rose and Mt Philp Breccias (e.g. Blake et al., 1982; Ryburn et al., 1988a and b). These breccias are extremely diverse in morphology, and their genesis remains poorly understood. An association between brecciation and alteration indicates the presence of hydrothermal fluids and suggests an important role for elevated fluid pressure in driving brecciation. In the Eastern Succession (Figs. 4.1 and 4.2), some of these breccias are clearly fault-hosted (e.g. Davis, 1997; **Chapter 5, this study**), and/or formed in the roof zones of late-tectonic intrusives (e.g. Mark and Foster, 2000). Elsewhere the breccias are apparently distal to fault zones and intrusive bodies. In many cases the breccias appear to be related to folding of complexly

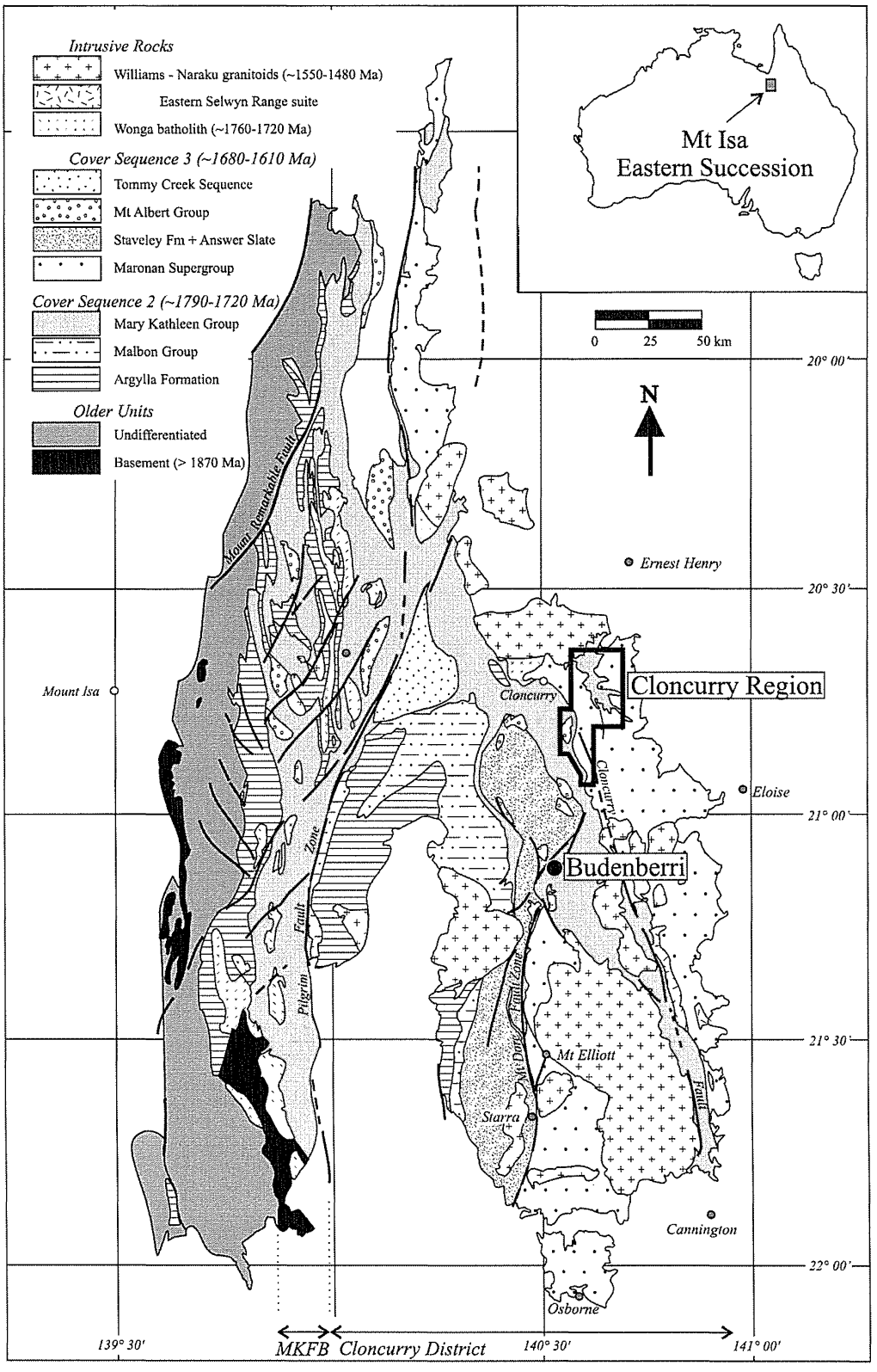

FIGURE 4.1.
Simplified geology of the Eastern Succession of the Mt Isa Block. Modified after Williams (1998).

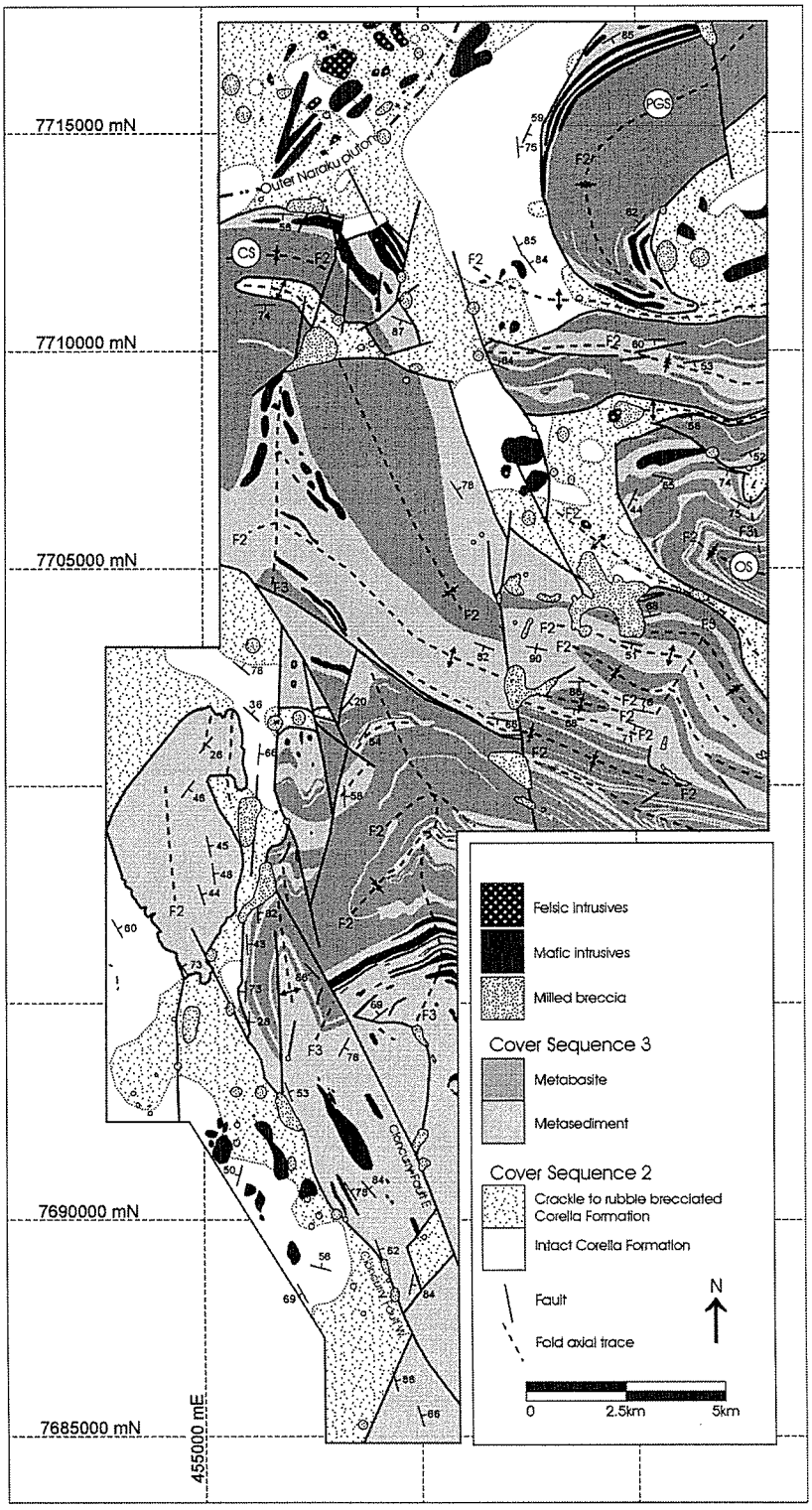

FIGURE 4.2.
Geological map of the Cloncurry Region, highlighting the widespread distribution of brecciation in the Corella Formation (Cover Sequence 2). CS = Cloncurry Syncline, PGS = Pumpkin Gully Syncline, OS = Oonoomurra Syncline. Note widespread brecciation in the roof zone of the Outer Naraku pluton, along some NE to NW trending fault segments, as well as distal to intrusives and fault zones. The largest zones of intact Corella Formation stratigraphy, for example west of the Pumpkin Gully Syncline, are characterized by predominantly NS trending stratigraphy.

fractured and boudinaged rocks. The aim of this chapter is to document evidence for the local control of buckle folding and resultant stress fields on the development of brecciation in the Eastern Succession, with the understanding that the dominant driving mechanism for brecciation may be elevated fluid pressure. It is not possible, nor does this chapter aim to attribute all brecciation in the Eastern Succession to a single structural mechanism. Rather the focus here is to make a case for the little documented relationship between folding and brecciation processes.

4.1.1 Terminology and classification schemes

The development of folds of different styles reflects a range of parameters, including the temperature and pressure conditions during folding, the relative strength of rock layers, and the deformation mechanism(s) active during folding. The informal term 'competence' is used here to describe the relative strength of rocks, and is a reflection of the extent to which a material is able to resist plastic flow at a given differential stress. Thus, at a given stress, an 'incompetent' material flows more readily than a 'competent' material, and a competent material is in turn more prone to fracturing. Adjacent rock layers of different competence may exhibit different fold and/or fracture styles during the same deformation event. Conversely, the same rock layer can exhibit different fold styles when deformed under different conditions.

In this chapter, the dip-isogon based fold classification scheme of Ramsay (1967) is employed (Fig. 4.3a), as well as plots of the relative orthogonal thickness versus the angle of dip (t'α vs. α plots; see Fig.4.3b for fold parameter definitions). In some instances dip isogons have been drawn on surfaces that are non-orthogonal to the fold axis (e.g. map views of moderate to steeply plunging folds). In these cases, isogon plots cannot be used to assign folds to Ramsay's fold classes, but are still useful in comparing the relative convergence and divergence of isogons across adjacent layers, provided that the relation between the observed surface and the fold axis is constant.

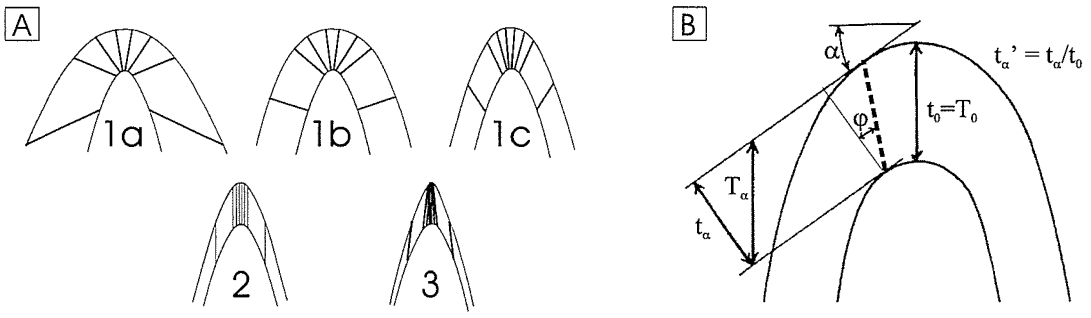

FIGURE 4.3.
(a) Geometric fold classes of Ramsay (1967). Class 1b folds are 'parallel folds' and Class 2 are 'similar folds.' (b) Geometric relationship of variables used in describing fold shape, including: orthogonal thickness (t_α, t_0 at the fold hinge), thickness parallel to the axial surface (T_α, T_0 at the fold hinge), dip isogon angle (φ) and fold surface dip angle (α). The dashed line indicates a dip isogon connecting points of equal slope on adjacent fold surfaces. Modified after Ramsay (1967).

The geometric boudin classification scheme of Goscombe and Passchier (2001, 2003) has been adopted in this study. Boudins are subdivided into drawn, torn, domino, gash and shearband classes (Fig. 4.4).

In this and subsequent chapters, breccias are described in terms of three components: clasts, matrix and infill (Taylor and Pollard, 1993). Clasts are fragments of rock derived through fracturing, and in this study the term is reserved for fragments greater than 1mm in size. Two varieties of matrix are distinguished. The first, here simply termed 'matrix' is made up of comminuted rock fragments less than 1mm in size. This is distinguished from 'marble matrix' that consists of calcite-rich marble that shows no mesoscopic evidence for fracturing, and is inferred to have filled dilational gaps between boudins and/or clasts by plastic flow. Infill is material precipitated into open spaces from hydrothermal fluids, and is here predominantly represented by calcite, quartz and actinolite in varying proportions.

The qualitative terms crackle, mosaic, rubble and milled are used in describing a progression in the physical characteristics of brecciated rocks. The use of these terms is not intended to carry any genetic connotation. Crackle breccias exhibit interconnected networks of fractures. Clasts are in situ, angular and non-rotated. Bedding and early formed fabrics (where present) are readily traced through the zone of brecciation. Mosaic breccias exhibit well-developed interconnected fracture networks. Clasts are in situ, typically sub-angular, and exhibit some degree of rotation. Individual bedding layers and foliations may become obscured, but major stratigraphic boudaries (where present) are traceable through the zone of brecciation. Rubble breccias are characterized by variable, but predominantly rounded and rotated clasts, and often contain a significant matrix component. Only major stratigraphic boundaries can typically be traced through the breccia zone. Milled breccias contain variable, but commonly well-rounded clasts, and layering is not traceable through zones of brecciation. These breccias are commonly polymictic, and in places clast lithologies do not match the immediate wallrocks. A significant matrix component is typically present.

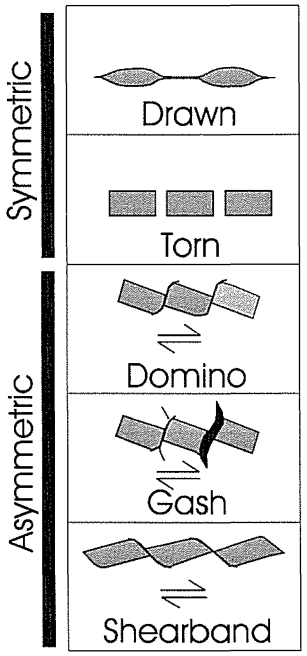

FIGURE 4.4.
Geometric boudin classification scheme of Goscombe and Passchier (2001, 2002). Both torn and drawn boudins are symmetric, but torn boudins show blocky clasts indicative of predominant fracturing, while drawn boudins have tapered shapes, indicative of plastic flow. Domino boudins are asymmetric and blocky, and inter-boudin surfaces form at high angles (typically >58°) to the bounding surface, and commonly exhibit dilation between clasts. Gash boudins differ from domino boudins in having inter-boudin surfaces with sigmoidal or branching traces. Shearband boudins are asymmetric, have tapering shapes, and inter-boudin surfaces form at low angles (typically <58°) to bounding surfaces.

4.1.2 Buckle folds and accommodation structures

Buckle folds result from the application of the principal compressional stress subparallel to layering in sequences in which alternating layers are marked by significant differences in rheologic properties (e.g. Biot, 1965; Ramberg, 1963; Hudleston and Lan, 1994). Buckle folding commonly produces 'parallel' folds (Van Hise, 1896), where layers maintain a constant thickness throughout a fold. In contrast, passive folding is marked by 'similar' folds (Van Hise, 1896) that maintain a consistent shape from layer to layer. While similar folds can be infinitely propagated along a fold's axial plane perpendicular to the fold axis, parallel folding results in space problems that can be accommodated through a variety of mechanisms. In some cases, less competent layers (where present) will deform in such a way as to solve the space problems created by Class 1 folds developed in competent layers. For example, it has commonly been noted that layered rock sequences showing alternating Class 1 and Class 3 folds, in more and less competent layers respectively, display an approximate overall Class 2 fold shape (e.g. Ramsay, 1967; Zagorčev, 1993). In cases where either there is not enough incompetent material, or the incompetent material is too viscous to effectively accommodate space problems, other mechanisms may operate. Commonly recognized accommodation structures include saddle reefs, décollement surfaces, inner arc thrusts and fold-limb faults and shears (e.g. Ramsay, 1967; Price and Cosgrove, 1990; Windh, 1995).

4.1.3 Cloncurry District Geology

Much of the Eastern Succession of the Mt Isa Block, including large portions of the Cloncurry District and Mary Kathleen Fold Belt (Fig. 4.1), is dominated by calc-silicate rocks, metasiltstones, and mafic and felsic meta-volcanic rocks of the Mary Kathleen Group, including the Corella and equivalent formations (Cover Sequence 2: ca. 1790 to 1720 Ma). Voluminous granitoids and associated gabbro and dolerite of the Burstall and Wonga suites intruded these rocks at ca. 1760 to 1720 Ma. In the Cloncurry District, deposition and extrusion of siliciclastic metasediments and mafic amphibolites including the Soldiers Cap Group (Cover

Sequence 3: ca. 1680 to 1620 Ma) postdates Wongan aged plutonism. Both Cover Sequences 2 and 3 were metamorphosed at greenschist to amphibolite facies at ca. 1600 to 1570 Ma, and were subsequently intruded by the Williams and Naraku batholiths (ca. 1550 to 1500 Ma).

Here, the deformation sequence outlined in **Chapter 2** is briefly reviewed. Complex structural geometries in the Eastern Succession reflect the superposition of multiple folding and faulting events. During D_1, one or more sheets of Cover Sequence 3 rocks were emplaced (thrust?) over Cover Sequence 2 rocks, the contacts between the sequences being marked by shear zones. These sequences and shear contacts were subsequently folded by tight to isoclinal D_2 folds with a predominant N-S strike and steep dip. D_2 was broadly synchronous with the peak of metamorphism. Present variations in D_2 fold geometry reflect combinations of 1) strain partitioning around early intrusive bodies, 2) local strain accommodation by inferred reactivation of rift-related faults, 3) reorientation of D_2 folds by forceful displacement of wallrocks during intrusion of the Williams and Naraku batholiths, and 4) refolding under retrograde conditions during D_3. Significant ambiguity exists in distinguishing between these causes of regional variations in the orientation of D_2 folds, but such a distinction is not critical for the purposes of this chapter. The resultant complex fold patterns are offset by a well-developed syn- to post- D_3 fault array.

4.2 CLONCURRY DISTRICT STRUCTURAL OBSERVATIONS

4.2.1 D_2: Soldiers Cap Group

D_2 folds within micaceous metasediments and amphibolites of the Soldiers Cap Group are tight to isoclinal and closely approximate Class 2 folds. Hinge thickening is evident in all rock types. These folds are also characterized by a well-developed axial planar cleavage, which shows limited refraction across lithologic contacts. Fold trains contain adjacent waveforms with similar wavelengths, amplitudes and fold shapes. Mesoscale (<10m wavelength) folding of Soldiers Cap Group rocks is rare, while macroscale folds are readily identified, with amplitudes and wavelengths on the order of hundreds of metres to kilometres (Fig. 4.5).

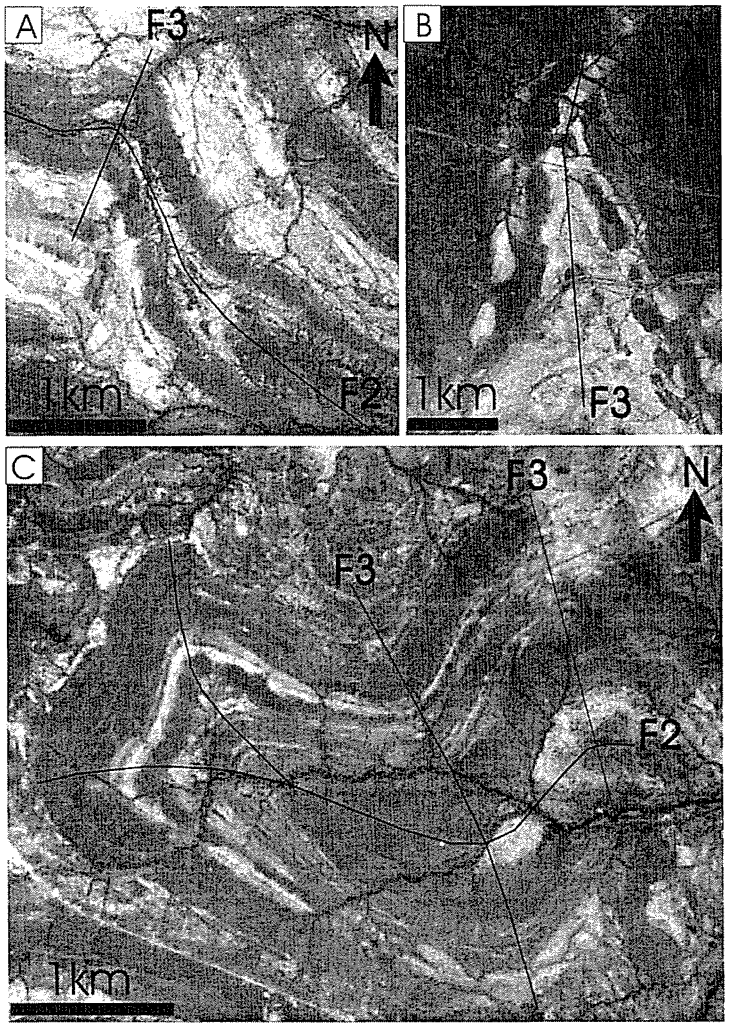

FIGURE 4.5.
D_2 and D_3 folds in the Soldier's Cap Group, reproduced from aerial photographs. Light coloured units are metasediments, dark units are metabasite and amphibolite. (a) Approximate location: 466500mE, 7701000mN. (b) Approximate location: 456500mE, 7708000mN. Segmentation of amphibolite unit is interpreted to represent pre-D_3 boudinage. (c) Oonoomurra Syncline. Aproximate coordinates: 468000mE, 7704500mN. All coordinates given in AMG, Zone 54.

Macroscale boudinage of thick (10 to 500m) metadolerite sills is locally evident, and boudins exhibit torn to drawn morphologies.

4.2.2 D_3: Soldiers Cap Group

D_3 folds are only locally developed within the Soldiers Cap Group. Folds commonly form isolated waveforms that die out up and down section (Fig. 4.2). Typical wavelength is on the order of hundreds of metres and mesoscale folds are rare. An axial planar crenulation cleavage is locally developed. Hinge zone layer thickening is noted in metasediments and metabasalts, but not in gabbroic to doleritic sills within the Soldiers Cap Group. Overall fold geometries tend to approximate Class 2 folds when layer effects are averaged out.

4.2.3 D_2: Corella Formation

D_2 folds within the Corella Formation are tight to isoclinal, and commonly exhibit a weakly developed foliation defined by the alignment of biotite grains, which shows minor refraction across bedding contacts. While hinge zone thickening is preferentially developed in calcite-rich layers, most stratigraphic layers show some degree of layer thickening at fold hinges (Figs. 4.6). Consequently, dip isogons drawn through sequences of bedded Corella Formation show weak convergence in siltstone and calc-silicate rock layers, and weak divergence in marble layers. Where layer effects are averaged out, isogon patterns typically approximate those of Class 2 folds (Figs. 4.6c).

Characteristic wavelengths and amplitudes are difficult to establish, due to the superposition of brecciation, but F_2 axial traces can in places be traced over distances of several kilometres. In intact thick-bedded calc-silicate and marble multilayers, F_2 wavelengths are on the order of 100m, and consistent fold shape, orientation and amplitude are repeated from one waveform to the next. Mesoscale folds are moderately common in more thinly bedded horizons.

Calc-silicate rock layers on the limbs of D_2 folds commonly exhibit pinch and swell structures and/or symmetric drawn boudins with rounded and tapered margins (Fig. 4.6a,b). Also common are boudinaged calc-silicate rocks with blocky

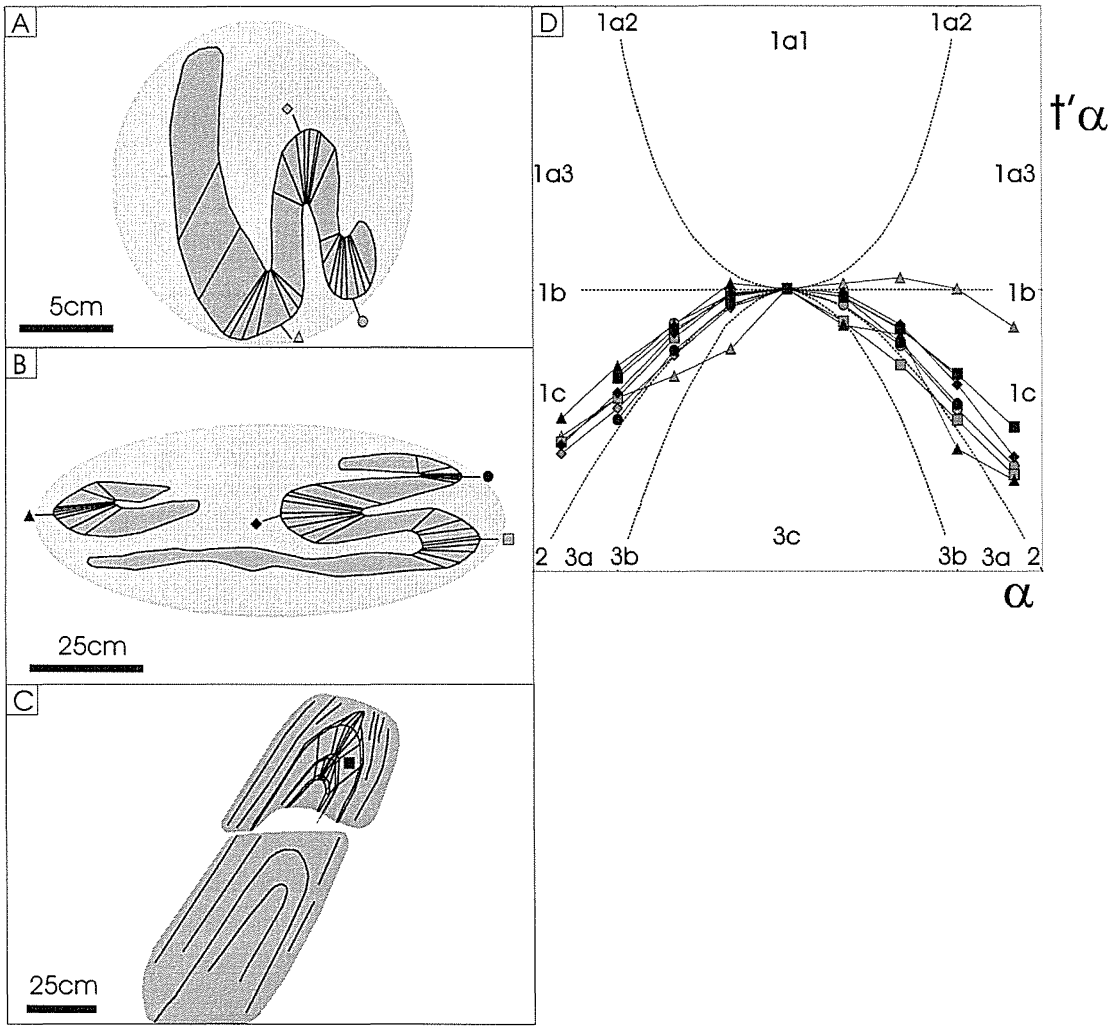

FIGURE 4.6.
(a-c) Line drawings with dip isogons from photographs of profile sections through D_2 folds in the Corella Formation. Symbols correspond to fold hinges plotted in Fig. 4.6d. All layers exhibit hinge zone thickening / limb thinning, and most calc-silicate and siltstone layers approach Class 2 folds. Note drawn boudins developed along fold limbs in Figs. 4.6a and b. (d) t'α vs. α plot for layers indicated in Figs. 4.6a, b and c, with additional fields from Zagorcev (1993).

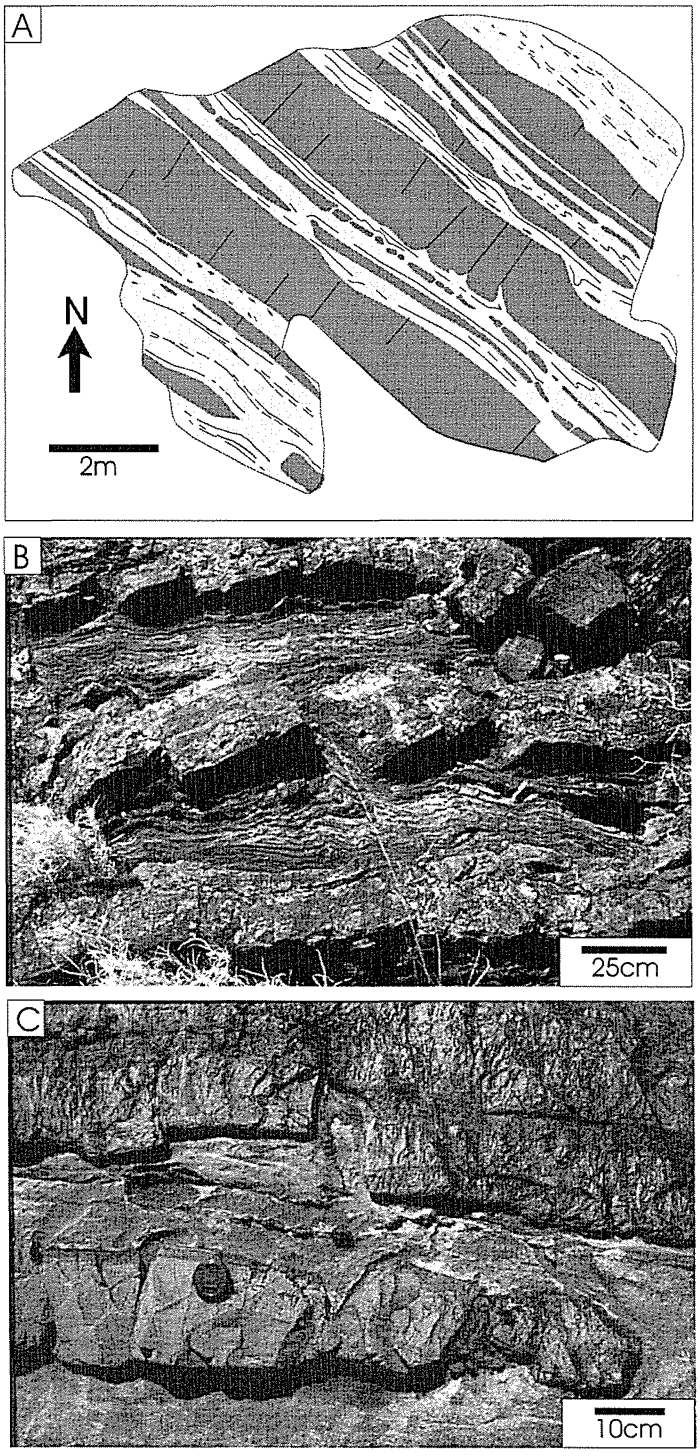

FIGURE 4.7.
Outcrop map and photographs of pre-D_3 boudins in marble and siltstone sequences in the Corella Formation. Map and photos at approximate coordinates: 466500mE, 7713200mN (AMG, Zone 54).

rectangular to trapezoidal boudins, with boudin margins defined by bedding contacts and layer-transecting fractures (Fig. 4.7). Both symmetric (torn) and asymmetric examples are noted. Asymmetric boudins are most commonly domino boudins, with inter-boudin surfaces formed by fracturing at high angles to bedding. Inter-boudin gaps contain a variable proportion of infill and marble which has flowed into boudin necks, commonly recorded by the presence of scar folds (Fig. 4.7). Chocolate tablet boudinage is locally noted, with both sub-vertical and subhorizontal extension evident. Marble horizons very rarely exhibit evidence for mesoscopic brittle failure.

Boudinage may have occurred either late during D_2 folding, as fold limbs were rotated into the extensional field, or during forceful displacement of folds in response to post- D_2 pluton emplacement. Correspondingly, the range in boudin morphology likely reflects boudinage under a range in ambient P-T-P_f conditions. Many boudin trains are clearly folded by D_3 folds (see below).

4.2.4 D_3: Corella Formation

D_3 folds in the Corella Formation are irregularly developed, and show limited continuity up- and down-section (Fig. 4.8b, 4.9a). Where adjacent waveforms are developed, these exhibit variable amplitude, wavelength, orientation and fold shape. Mesoscale folds are relatively common, and map-scale folds with wavelengths up to several kilometres are locally evident. Axial planar foliations are rarely identified.

Folded competent meta-siltstone and calc-silicate rock layers approximate Class 1b folds, and maintain a relatively consistent layer thickness throughout (Figs. 4.8 and 4.9). Less competent marble layers, where present, commonly exhibit significant hinge zone thickening, and reflect Class 2 to Class 3 fold shapes. Dip isogon patterns are highly irregular, typically exhibiting significant convergence in meta-siltstone and calc-silicate rock layers, and divergence in marble layers. Locally, where layer effects are averaged out, isogon patterns may approach those of Class 2 folds, but more commonly a gross convergence of isogons towards the inner arc of folds is seen.

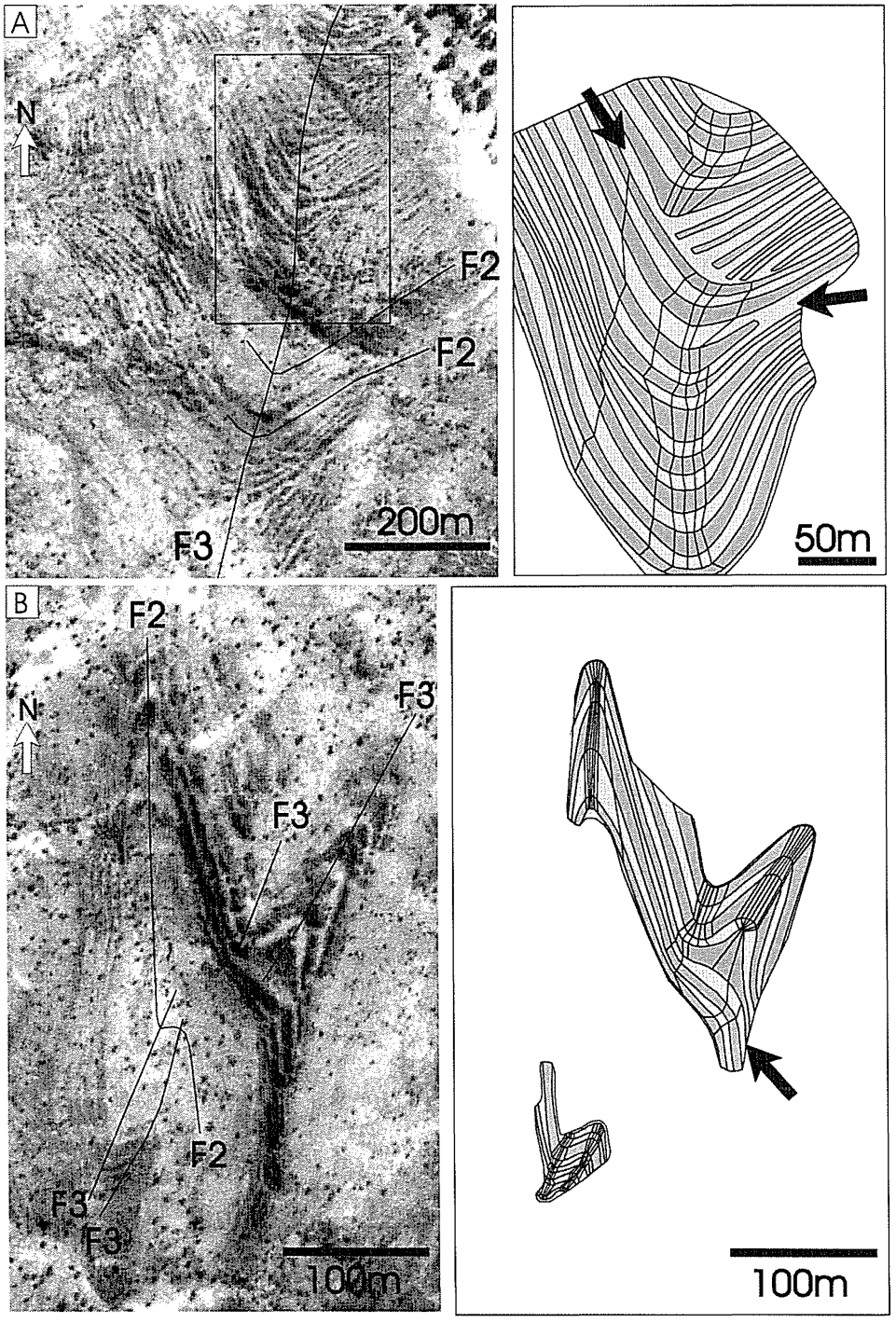

FIGURE 4.8.
Aerial photographs and line drawings with dip isogons of D_2 and D_3 folds in the Corella Formation. Hinge zone layer thickening is slightly exaggerated as a result of the images not being profile sections through the folds. (a) Truncation of bedding layers near D_3 fold hinges is interpreted to record fold-limb faults. Approximate location: 453500mE, 7695700mN. (b) Décollement zone in D_3 fold hinge. Approximate coordinates: 456700mE, 769000mN (AMG, Zone 54).

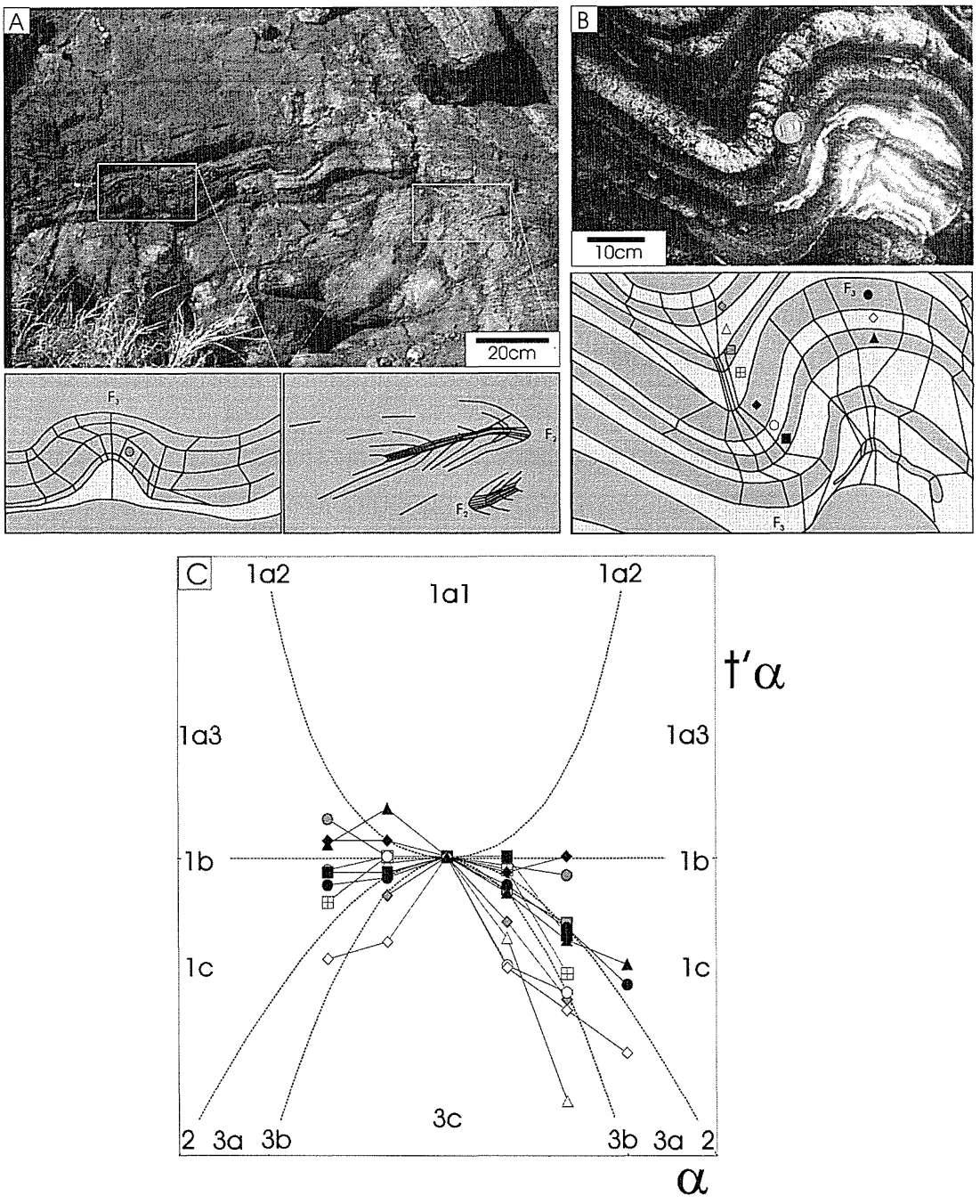

FIGURE 4.9.
(a-b) Line drawings with dip isogons from photographs of profile sections through D_3 folds in the Corella Formation. Symbols correspond to fold hinges / layers plotted in Fig. 4.9c. Black and grey symbols = calc-silicate rocks / siltstones, white symbols = marble. Hinge thickening is preferentially developed in marble layers. Note the décollement zone in Fig. 4.9a. (a) Approximate coordinates: 447500mE, 7693700mN (AMG, Zone 54). (b) Approximate coordinates: 464200mE, 7707600mN (AMG, Zone 54). (c) t'α vs. α plot for layers indicated in Figs. 4.9a and b, with additional fields from Zagorcev (1993).

While in many cases D_3 folds are imposed on previously fractured and boudinaged rocks, in some cases fractures are preferentially developed on one limb of D_3 folds (Fig. 4.9b). Elsewhere, the geometry of fracture sets resembles that predicted for fracture cleavage (e.g. Knill, 1960), and unfolding of D_3 folds reveals an asymmetry to fractures that is inconsistent with fracturing having entirely pre-dated folding (Fig. 4.10a). In other examples, extensional fractures have developed predominantly in the outer arc of meta-siltstone and calc-silicate rock layers (Fig. 4.10b). Combined these observations support a syn- or post- D_3 timing for some fractures. A syn-folding timing is inferred for many of these features, as buckle-related strain appears to have been in part accommodated by displacement across the fractures. Fractures are almost always confined to calc-silicate and siltstone horizons, with marbles rarely recording mesoscopic fracturing. As illustrated in Figure 4.10c, syn-folding fractures may develop as cleavage fractures (Knill, 1960; Hobbs et al., 1976), as interconnected outer-arc extension fractures and inner arc shear fractures (e.g. Ramsay, 1967), or as extension fractures which propagate through competent layers by means of effective layer thinning or volume gain folding (**Chapter 3**, this study).

4.3 FOLDS, FRACTURES, BOUDINS AND BRECCIAS

In this section, boudin and fracture characteristics are further described within Corella Formation stratigraphy. In many cases, fracturing can only be constrained to being pre- to syn- D_3, and in some cases multiple fracture sets are recognized, and early formed fractures may have been reactivated. Regardless of this relative timing, fractures appear to have played a significant role in the development of irregular D_3 fold geometries and breccia bodies.

4.3.1 Folded boudin trains and boudin rotation

Boudins formed in thin (<10cm) siltstone or calc-silicate rock horizons embedded in marble tend to maintain their original shape. This is typically rectangular to trapezoidal (i.e. torn, domino or gash boudins), governed by the original layer margins (i.e. bedding surfaces) and spacing of inter-boudin fractures.

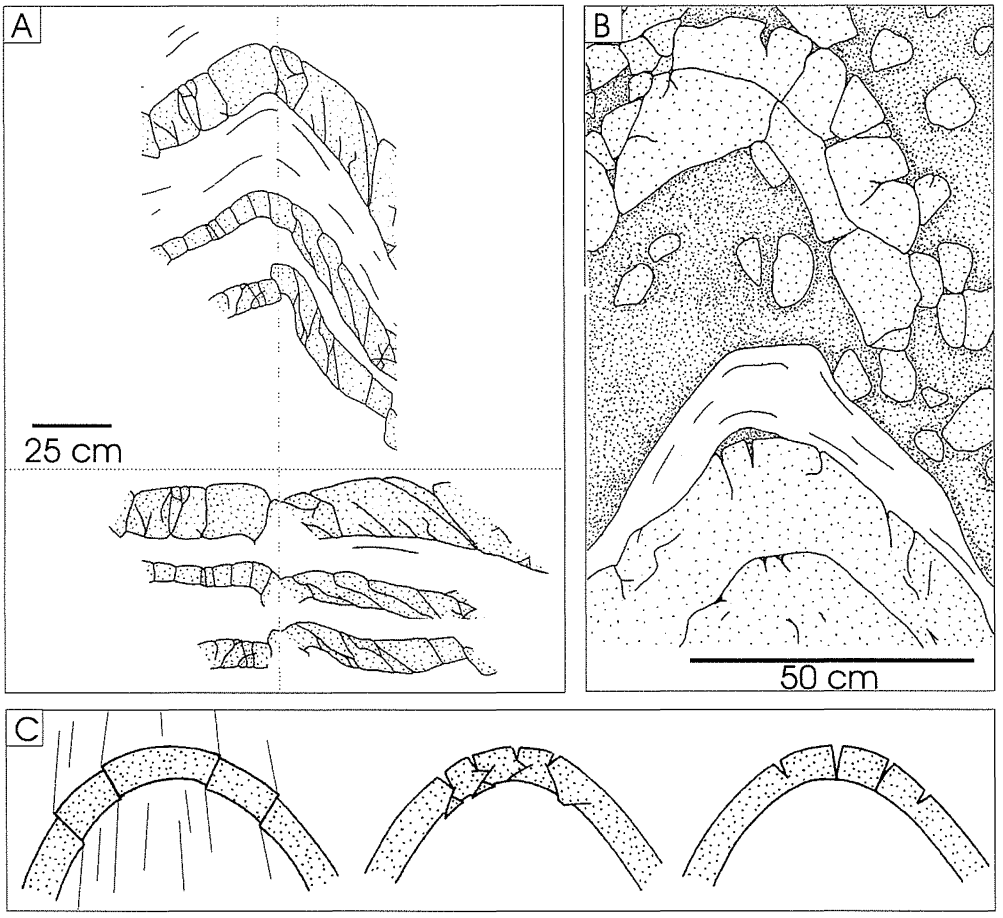

FIGURE 4.10.
(a) Line drawing from a photograph of D_3-folded calc-silicate (stippled) and marble (unornamented) stratigraphy. When unfolded by simple rotation across the fold hinge, fractures reveal an asymmetry which is inconsistent with all fractures forming pre-D_3, and indicate a syn- or post-D3 timing for some fractures. Approximate coordinates: 466500mE, 7713200mN (AMG, Zone 54). (b) Line drawing from a photograph of D_3-folded meta-siltstone (light stipple) and impure marble (unornamented) stratigraphy. Note development of extensional fractures in the outer arc of meta-siltstone layers, and brecciation (heavy stipple). Approximate coordinates: 448600mE, 7693800mN (AMG, Zone 54). (c) Theoretical models for the development of fold-related fractures include fracture cleavage (left), interconnected outer arc extensional fractures and inner arc shear fractures (middle), and through-going extensional fractures (right).

Where fractured and/or boudinaged meta-siltstone and/or calc-silicate rocks interbedded with marble were folded about D_3 folds, highly unusual geometries are preserved. Inferred processes include rotation of calc-silicate clasts to accommodate hinge zone outer arc extension, layer bound thrust faults in some buckled competent layers, and a general progression towards a chaotic arrangement of meta-siltstone and calc-silicate rock clasts within a marble matrix that shows no evidence for macroscopic fracturing (Fig. 4.11). Where layers are disaggregated to the point that stratigraphic layering is no longer recognizable, these rocks are referred to here as marble matrix breccia, an informal term originally defined for similar rocks in the footwall of the Ernest Henry Fe-oxide-Cu-Au deposit.

Clear evidence for rotation of many boudins is recorded by varying orientations of bounding surfaces for individual boudins (typically bedding surfaces) relative to the boudin train enveloping surface (Fig. 4.12a,b).

4.3.2 Brecciated multilayers

In meta-siltstone and calc-silicate multilayers, fracture networks or crackle breccias are commonly developed, with clast margins defined by fractures near-orthogonal to bedding, and by bedding margin fractures (Fig. 4.12c,d). Clasts in these multilayer crackle breccias resemble domino boudins seen in isolated meta-siltstone layers. A gradation is noted from these multilayer crackle breccias with minor clast or boudin rotation, to statabound mosaic, rubble and milled breccias (Fig. 4.12e,f).

Clasts within stratabound mosaic to milled breccias are monolithic and appear to have been derived from within the horizon in which they are found. Clasts exhibit highly variable shapes with rectangular and trapezoidal clasts (resembling domino boudins) as well as progressively more rounded morphologies present. Material in between clasts contains a variable proportion of finely comminuted clast-derived matrix, fine-grained marble matrix and coarse-grained calcite-dominated infill. Locally, clasts and comminuted matrix are variably altered to albite- and actinolite-rich mineral assemblages of inferred hydrothermal origin. Elsewhere, the breccia matrix minerals are in mineralogical and isotopic

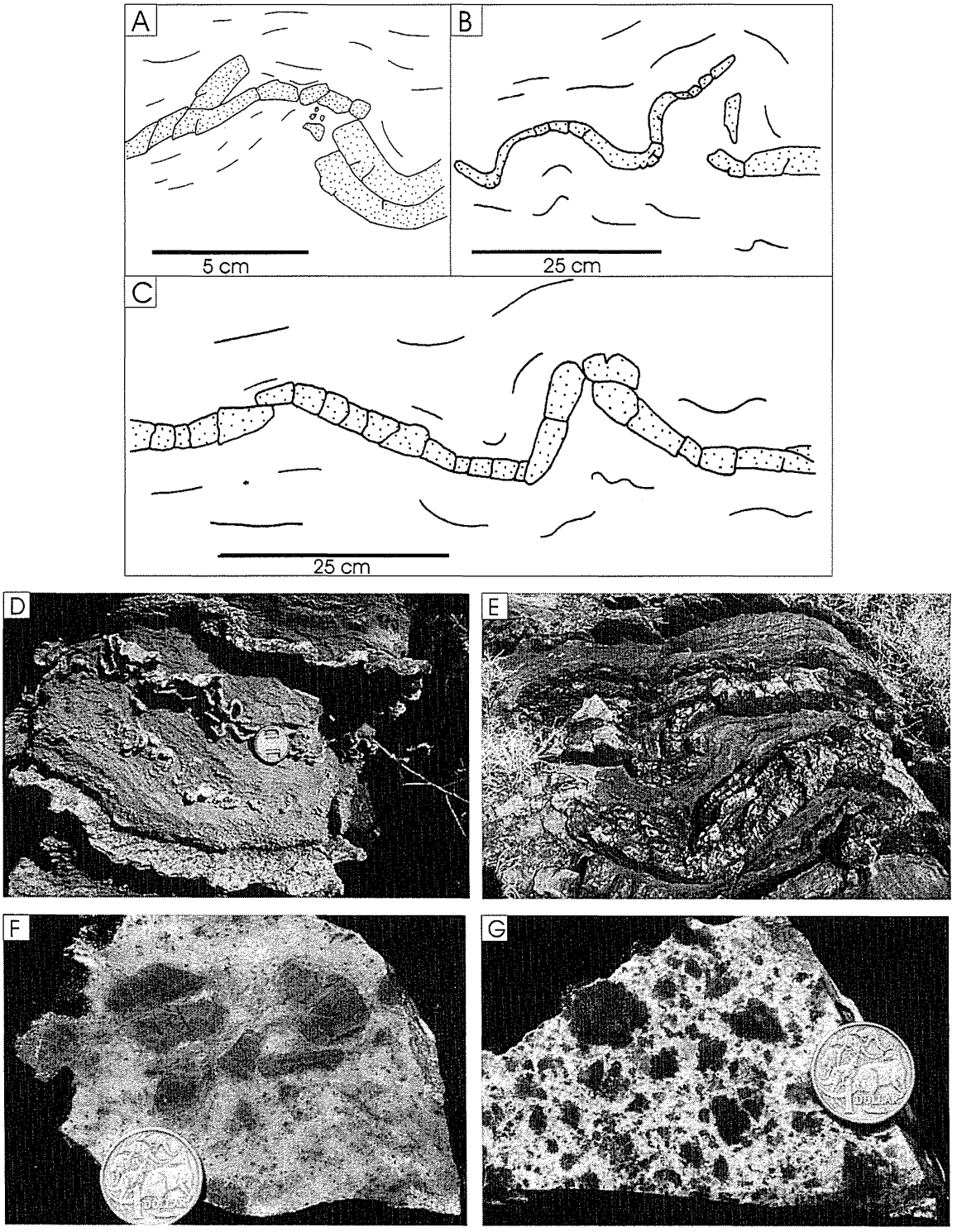

FIGURE 4.11.
(a-e) Line drawings from photographs, and photographs illustrating features produced by folding of boudinaged and fractured rocks, including: layer bound thrusts, highly irregular fold patterns and a progression towards a chaotic arrangement of calc-silicate and siltstone clasts in marble. Examples are from throughout the Cloncurry Region. (f-g) Photographs of hand specimens of marble matrix breccia. Diameter of coin is 2.4cm.

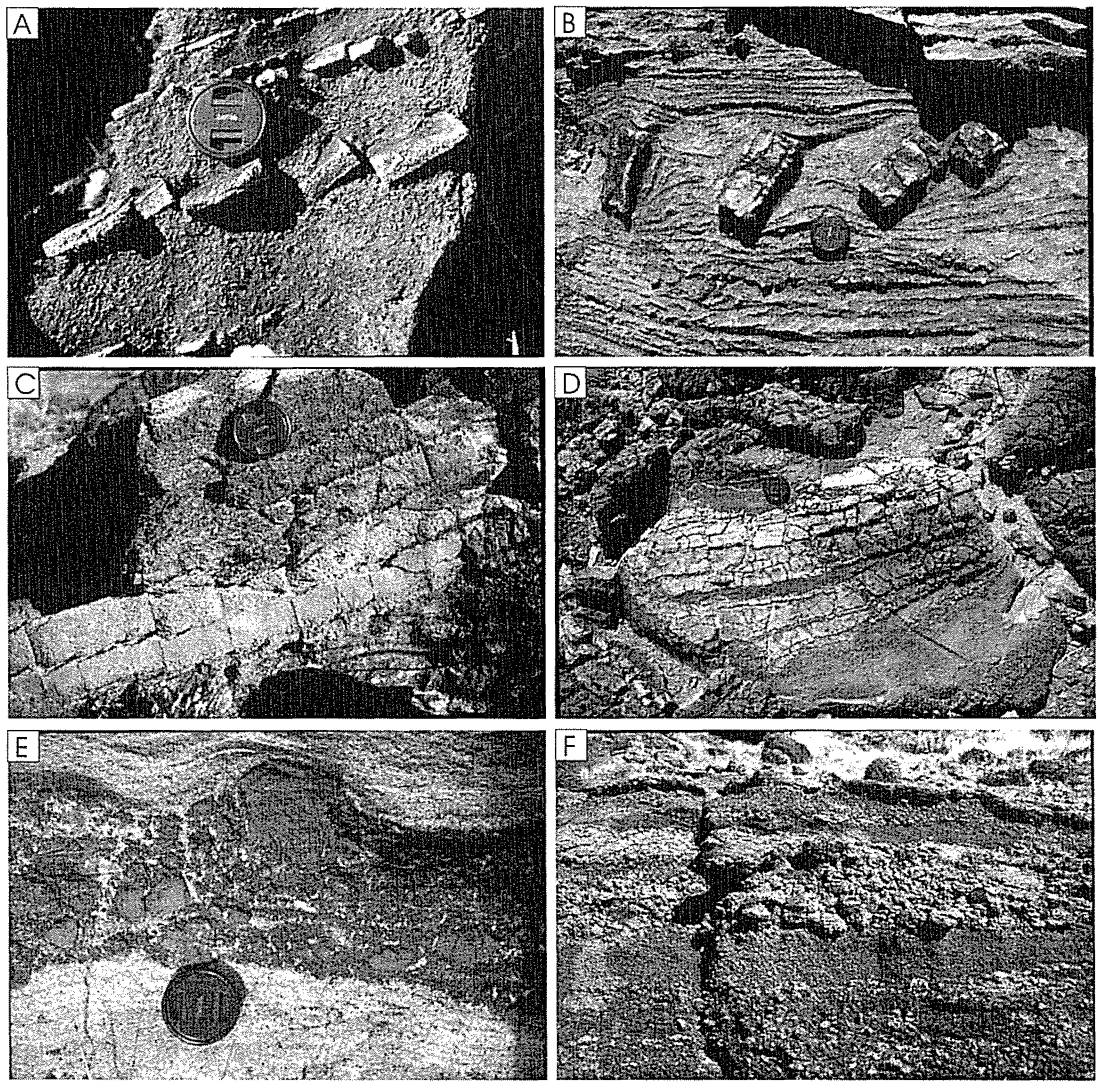

FIGURE 4.12.
Fracturing, boudinage and brecciation in the Corella Formation. Photos are from various field locales throughout the Cloncurry Region. Diameter of lens cap in all photos is 5cm. (a-b) Rotated domino boudins in isolated calc-silicate horizons within thicker marble units. (c-d) Crackle brecciation in calc-silicate multilayers. Fractures are dominantly bedding orthogonal and bedding parallel, and extend through individual layers, with clasts resembling domino boudins. Only minor clast rotation is evident. (e-f) Mosaic to milled stratabound breccias.

equilibrium with unaltered Corella Formation lithologies (i.e. calcite, quartz, biotite and K-feldspar assemblages; **Chapters 6** and **7**, this study).

Stratabound breccia bodies vary widely in size and structural position. Brecciated horizons range from ~5cm to tens of metres in width (Figs. 12e,f). Breccia bodies are noted both along D_3 fold limbs and in fold hinges (Fig. 4.13). Locally the breccias cut stratigraphic layering at shallow angles or are interconnected with veins and breccia dykes oriented approximately normal to bedding (Fig 4.13).

4.3.3 Accommodation structures

Accommodation structures are commonly associated with D_3 folds in the Corella Formation, and include décollement zones (Fig. 4.9a) and fold-limb faults (Fig 4.8a). Also noted are hinge-zone breccia bodies which narrow or pinch out along fold limbs (Fig. 4.10b, 4.13). The crescent-shaped geometry of these breccia bodies resembles saddle-reef structures.

4.4 DISCUSSION

The above observations reveal a consistent temporal evolution in structural style in the Corella Formation. D_2 folds exhibit consistent wavelengths and amplitudes, significant hinge thickening in all rock types, and moderately well developed near axial planar cleavage. In contrast, D_3 folds are highly irregular and fold related foliations are rarely evident. Retrograde deformation during D_3 was accommodated in large part by flow of low competence calcite-rich units. Competent siltstones and to a lesser degree calc-silicate rocks exhibit negligible hinge zone thickening, and appear to have been unable to accommodate significant intercrystalline plasticity or diffusive mass transfer (ie. ductile strain) during D_3. Late D_2 to syn- D_3 fracturing and boudinage of siltstones and calc-silicate rocks segregated originally continuous competent layers into isolated rigid blocks around which less competent material was able to flow.

A morphological continuum from crackle breccia or incipient boudinage with minor clast rotation in multilayers, to mosaic and milled stratabound and

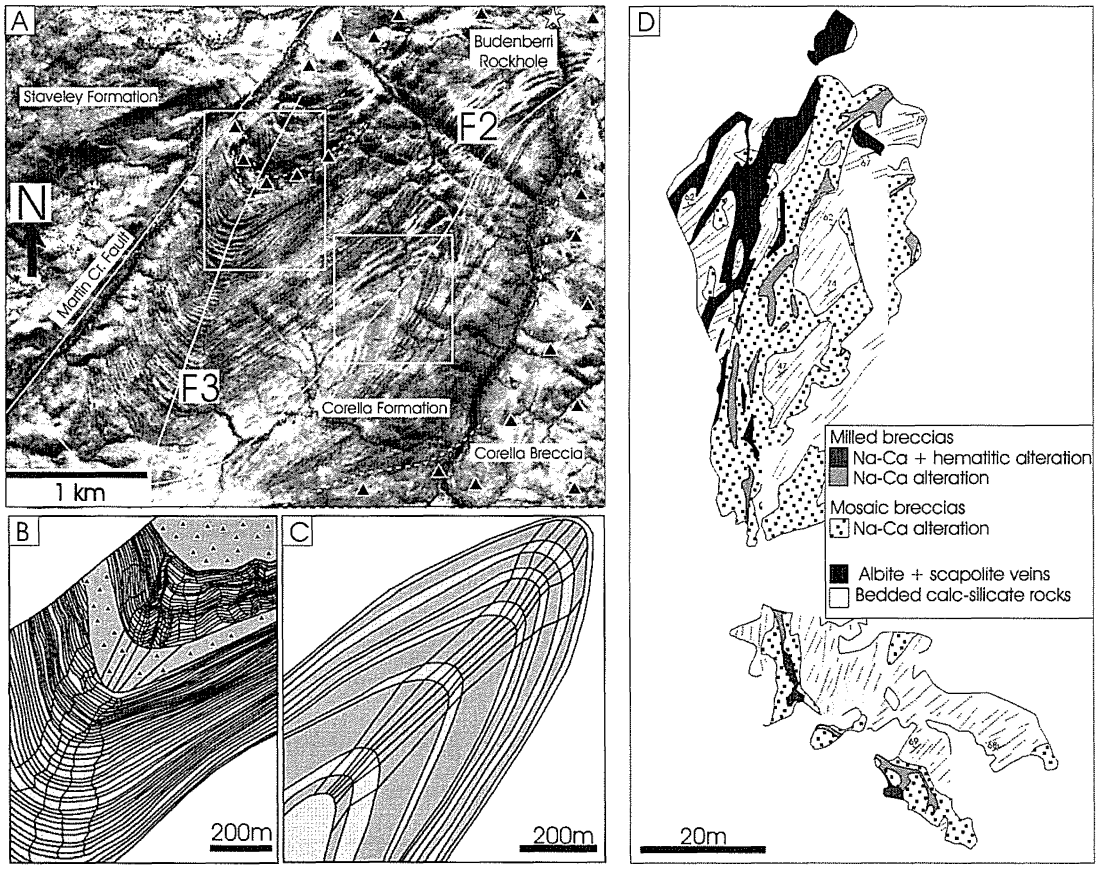

FIGURE 4.13.
(a) Aerial photograph and mapped geology of D_2 and D_3 folds in the Budenberri Region. Note the hinge zone, saddle-reef style breccia body (triangle pattern). (b-c) Dip isogon plots for the folds in Figure 4.13a. The two macroscopic fold axes have different trends, but nearly identical plunges allowing for a relative comparison of dip isogon profiles. The D_2 fold shows far less convergence and divergence in isogon patterns than is seen in the D_3 fold. Both marble (light grey) and calc-silicate rock (dark grey) layers in the D_2 fold more closely approximate Class 2 fold shapes than identical layers in the D_3 fold, which more closely approximate Class 3 and Class 1b shapes respectively. (d) Outcrop map of the Budenberri Rockhole illustrating the development of both stratabound and discordant bodies of the Corella Breccias.

discordant breccias is noted. Extreme rotation of boudins in isolated meta-siltstone horizons is also documented, and it is proposed that rotation of boudins or clasts in multilayers resulted in cataclastic grinding between clasts to produce stratabound breccia bodies. Consequently, original boudin morphology in multilayers is retained only where minor rotation has occurred. In contrast, domino boudins developed in isolated competent layers commonly maintain their original blocky morphologies, as cataclasis between rigid clasts did not occur, even with significant rotation.

Boudin rotation both in single layers and multilayers was likely in response to shear stress acting across the layers (Fig 4.14a,b; see also Goscombe and Passchier, 2003). Shear stress can be explained in the context of oblique compression across rotating fold limbs during buckle folding being translated into layer parallel and layer normal components (Fig. 4.14c). Where bedding-orthogonal fracture zones have developed, either pre-or syn-buckling, then a component of bedding orthogonal shear may result in shear across these zones, leading to cataclasis and brecciation, producing discordant breccia bodies (Fig. 4.14d). Fold limb rotation would also result in rotation of early-formed fractures relative to the bulk shortening vector. As a consequence, early extensional fractures may be reactivated as shear fractures and vice versa, greatly assisting in the brecciation process (see also Ismat and Mitra, 2001).

4.4.1 Brecciation as an accommodation mechanism

A number of authors have investigated the role of cataclasis in producing deformation features which record uniform flow at outcrop and broader scales (e.g. Stearns, 1968; Hadizadeh and Rutter, 1983; Blenkinsop and Rutter, 1986). At broad scales, cataclasis can be considered as a ductile process, despite being the product of fragmentation at finer scales. For example, Ismat and Mitra (2001) proposed cataclastic flow as a mechanism for fold limb rotation and thinning, allowing for progressive fold tightening in the shallow crust. The authors demonstrated that collective brittle movement on fracture networks resulted in homogenous and continuous flow that resembled ductile deformation at the outcrop and broader

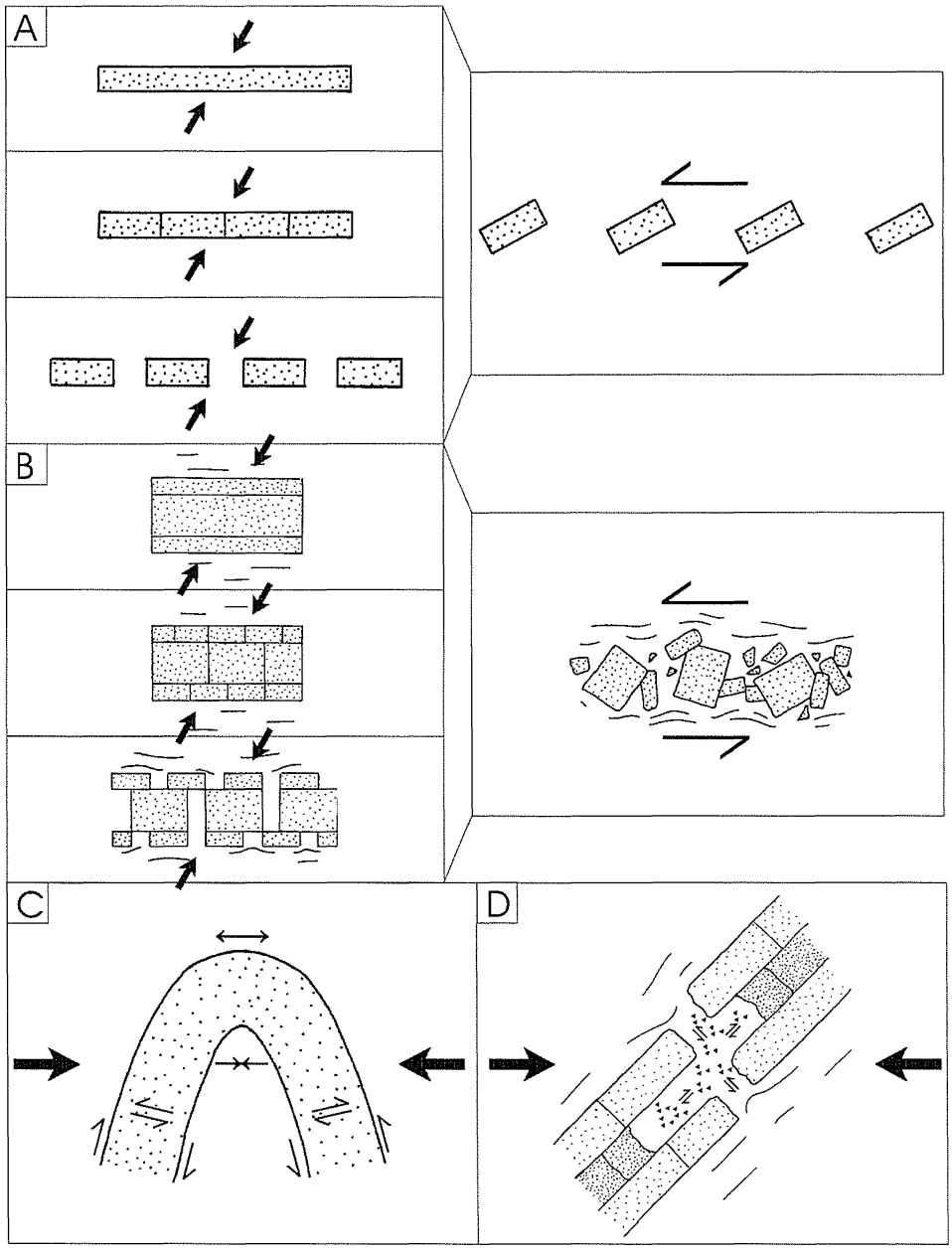

FIGURE 4.14.
Schematic diagrams illustrating inferred brecciation mechanisms, based on field observations in the Cloncurry District. (a) Sketch illustrating three initial layer geometries (intact, fractured and boudinaged) subjected to layer oblique compression (left). Arrows indicate the orientation of σ_1. Rotated boudins in the final geometry (right) may be produced from any of the three indicated initial geometries, highlighting the ambiguity of determining initial geometry, and the timing of fracture genesis. (b) Sketch illustrating boudin rotation in a multilayer in response to shear induced by layer oblique compression, for three possible initial geometries (left). Rotation of boudins in a multilayer sequence may result in cataclastic grinding and brecciation. (c) Simplified illustration of the local stress field associated with buckle folding, including outer arc extension, inner arc compression and resolution of oblique compression acting on fold limbs into layer parallel and layer normal shear components. (d) Schematic illustration of the development of layer parallel and layer normal shear stress across a multilayer, located for example, on a fold limb, as in Fig. 4.14c. Resultant shear stresses may lead to cataclasis along layer-normal fracture zones, and along competent lithologies, producing discordant and stratabound breccia bodies respectively. Triangle pattern represents resultant zones of cataclasis and brecciation, and does not necessarily imply dilation.

scales. A similar model is proposed for the Corella breccias in which collective movement along fracture zones and breccias records an effective decrease in the competence of originally stiff layers. One consequence of this is that where space problems associated with buckle folding could not be accommodated by flow of low competence marble towards fold hinges, competence reduction in siltstones and calc-silicate rocks by brecciation allowed for increased flow of these rocks, facilitating limb thinning and hinge thickening. Thus brecciation locally acted as an accommodation mechanism for space problems associated with D_3 buckle folding. Direct evidence for this can be found in crescent-shaped saddle-reef style breccia bodies (Figs. 4.10b, 4.13a,b).

In Figure 4.15, the minimum ratio of incompetent to competent material required in order to accommodate space problems developed during buckle folding is calculated. Where the proportion of different lithologies in a rock sequence does not meet this ratio, various accommodation mechanisms including brecciation may allow for further fold tightening. Figure 4.15 illustrates for example, that for the given input parameters (see figure caption), 30% layer shortening requires approximately 20% incompetent material in the buckled sequence. In theory, plots such as Figure 4.15 can be applied to natural examples, with estimates of layer shortening and the percentage of incompetent material in a sequence being plotted in order to estimate if accommodation structures will be necessary for fold propagation. However, a number of critical assumptions and difficulties in estimating layer shortening would hinder the use of such plots, particularly in complexly folded sequences. Nonetheless, Figure 4.15 highlights the near linear relationship between the minimum amount of incompetent material in a buckled sequence and the amount of layer shortening. This demonstrates the increasing likelihood of space problems developing during buckle folding at greater degrees of layer shortening, and in sequences with small ratios of incompetent to competent material. This may in turn explain why in some regions, such as the Spinifex area where marbles and calcite-rich calc-silicate rocks are common, D3 folding did not result in brecciation. In contrast, in the Budenberri area, fold-related brecciation is preferentially developed in certain stratigraphic packages, presumable those that had

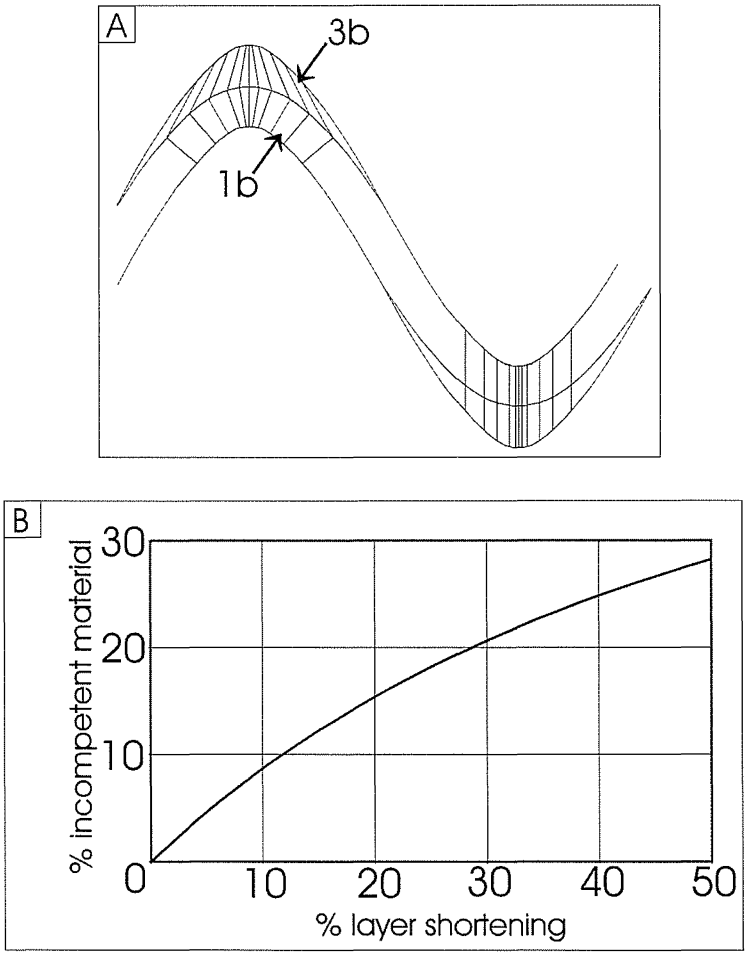

FIGURE 4.15.
(a) Sketch of Class 1b + Class 3b and resultant Class 2 folds, as defined by Zagorcev (1993). In the antiform, dip isogons have been drawn for the Class 1b and 3b folds, while in the synform, isogons have been drawn for the resulting Class 2 fold. The area of the Class 3b fold represents the minimum amount of incompetent material required to accommodate space problems associated with the Class 1b fold. (b) Plot illustrating the mimimum percentage of incompetent material required in a multilayer to accommodate the space problems associated with sinusoidal Class 1B folding of competent layers. The ratio $Area^{Class\ 3b}$: $Area^{Class\ 2}$ corresponds with the required amount of incompetent material for a given amount of layer shortening. Calculation of this ratio for sinusoidal folds is given in Appendix 4.A. Application of this calculation assumes that the incompetent material has a low enough viscosity to flow into the hinge zones at a rate which keeps pace with the folding, and the calculated area (and hence minimum percentage of incompetent material) will vary as a function of fold shape.

a low percentage of incompetent material. For example, brecciation is well developed at the Budenberri rockhole (Fig. 4.13), where no marbles are found in an approximately 100m thick stratigraphic package.

4.4.2 Contributing factors for brecciation in the Corella Formation

In this contribution, widespread breccias have been documented that exhibit a range in morphological characteristics. The breccias are largely restricted to forming during retrograde metamorphism, folding and synchronous pluton emplacement and are predominantly restricted to Corella Formation stratigraphy within the Cloncurry District. This implies controls on the genesis of the breccias that varied with time, space and lithology.

While stress, strain rate and pore fluid pressure all play a role in governing fold shapes developed in a given rock sequence, temperature also plays a critical role. For example, Parrish et al. (1976) demonstrated a strong temperature dependance on the quartzite : marble viscosity ratio, and hence on the development of parallel or similar folds. Because metamorphic mineral assemblages indicate that D_3 was retrograde relative to D_2 (e.g. Rubenach and Barker, 1998; Lewthwaite, 2000), temperature is inferred to have played a significant role in the varying fold morphologies between D_2 and D_3 observed in the Cloncurry District.

In the Mary Kathleen Fold Belt (MKFB) to the west of the Cloncurry District, Oliver et al. (1991) and Holcombe et al. (1992) document D_3 fold breccias in the Corella Formation, but these appear to be nowhere nearly as widespread as in the Cloncurry District. D_2 boudinage is more common in the northern Cloncurry District than the MKFB, and likely reflects greater effective competence contrasts as a result of lower D_2 temperatures in the northern Cloncurry District (ca. 550°C) relative to the MKFB (ca. 650°C). Reactivation of D_2 fractures, and folding of D_2 boudinaged layers during D_3 would thus be more widespread in the Cloncurry District. Additionally, D_2 fold limbs had a relatively consistent N-S orientation at the onset of D_3 in the MKFB, such that D_3 inferred E-W directed shortening was largely accommodated by reactivation of D_2 structures, as opposed to refolding. Similarly in the Cloncurry District, the largest areas of non-brecciated Corella

Formation stratigraphy also contain predominantly N-S oriented stratigraphy (Figs. 4.2 and 2.6), that was not appropriately oriented for D_3 buckle folding. Notably in the MKFB, D_3 folds and breccias are most abundant in D_2 strain shadows around competent intrusive bodies, where bedding was not oriented N-S at the onset of D_3 (Holcombe et al., 1992). Finally, late metamorphic intrusions are far more common in the Cloncurry District than in the MKFB, and likely resulted in a correspondingly more widespread increase in fluid pressure and transient strain rate variations that aided in fracturing. While elevated temperatures associated with pluton emplacement might be expected to counteract these effects, the abundance of brecciation in the roof zones of some plutons (Fig. 4.2; see also Mark and Foster, 2000) suggests that in these instances, increased strain rate and fluid pressure played a greater role than temperature in governing deformation style.

The Soldiers Cap Group is dominated by micaceous metasediments and amphibolites that preserve multiple generations of axial planar cleavages (e.g. Lewthwaite, 2000). Boudinage is comparatively rare, likely reflecting smaller competence contrasts than were active in the Corella Formation. Similarly, D_3 fold shapes suggest that folding in these rocks more closely approximated passive folding than D_3 folds developed in the Corella Formation, likely reflecting smaller competence contrasts between lithologies in the Soldiers Cap Group than in the Corella Formation. While some relatively competent layers in the Soldiers Cap Group exhibit Class 1 fold shapes (e.g. metadolerite sills), space problems associated with these appear to have been effectively accommodated by flow of voluminous incompetent schists.

Assessing the relative importance of the above factors in the brecciation process is an arduous task. In some areas, for example in the roof zone of the outer Naraku pluton (NW corner of Fig. 4.2), the inference can be made that elevated fluid pressure was the predominant factor driving brecciation. Such an interpretation is consistent with the corresponding occurrence of widespread metasomatic assemblages of inferred magmatic origin in this area (see **Chapter 6**). However, in many cases a structural control to the geometry of breccia bodies can be shown, and as such it is preferable to consider brecciation in the Eastern Succession (and

elsewhere) in terms of a continuum between tectonic and magmatic-hydrothermal breccia styles.

4.4.3 Implications for metasomatic fluid pathways

The widespread distribution of late-metamorphic brecciation in the Cloncurry District has implications for fluid flow pathways during pluton emplacement and broadly synchronous Cu-Au mineralisation. The fault valve model (Sibson et al., 1988) has been widely applied to explain fault-hosted mineralisation in a variety of mesothermal ore environments including some Cu-Au deposits of the Cloncurry District (Davis, 1997; **Chapter 5**, this study). The model provides a mechanism whereby metasomatic fluids may be focussed into narrow ore fluid conduits and depositional sites. However, in metamorphosed rocks the volume of fluid that can be sourced by the fault valve mechanism is limited by the low permeability of these rocks (e.g. Oliver, 2001). This can be overcome to some degree where faults are emplaced within broader high permeability fault-fracture meshes, out of which fluid can be drawn (e.g. Sibson, 1996; Sibson and Scott, 1998). However, a vertical limit is imposed on fault-fracture meshes by the tensile strength of overlying rocks (Cox et al., 1991; Sibson and Scott, 1998). This vertical limit imposes a significant restriction on the volume of rock out of which fluids can be sourced during fault valving.

The Corella breccias may have acted as a series of stacked fault-fracture meshes. The presence of interlayered low-permeability marble horizons that were not prone to throughgoing brittle failure, may have allowed for the development of stacked fault-fracture meshes over a total depth range greater than that imposed for a single mesh. Stacked fault-fracture meshes would thus effectively increase the volume of rock out of which fluid may have been drawn during fault valving. This concept is further explored in **Chapters 5** and **8**.

4.5 CONCLUSIONS

It is proposed that the geometric distribution of brecciation in the Cloncurry District is in part a function of the stress field active during buckle folding.

Retrograde folding was both synchronous with fracturing, and imposed on rocks that were already fractured and boudinaged. Locally this resulted in folded boudin trains with a chaotic breccia-like arrangement of clasts. Elsewhere, oblique shear imposed across fractured and boudinaged rocks resulted in rotation of boudins and clasts that is inferred to have caused cataclastic grinding, producing both stratabound and discordant breccias.

A morphologic continuum is noted between boudinaged and brecciated rocks, and similar genetic mechanisms are inferred for both. Further, it is proposed that fracturing, boudinage and brecciation resulted in a net reduction in the competence of some rock layers. This allowed for increased flow of initially stiff lithologies, which in part accommodated buckle-fold related space problems. Brecciation has not been previously documented in this manner as an accommodation structure. Conclusive evidence for this mechanism can be found in the Cloncurry District in the form of saddle-reef style breccia bodies.

In the Eastern Succession, a number of factors contributed to widespread brecciation that was largely confined to forming syn- D_3, and within Corella Formation rocks of the Cloncurry District. These include: 1) Lower D_2 temperatures in the Cloncurry District relative to the MKFB, promoting late- D_2 fracturing and boudinage; 2) Anomalous fold orientations in the Cloncurry District at the onset of D_3 (see **Chapter 2**, this study), favoring refolding, as opposed to predominant tightening of D_2 folds in the MKFB; 3) Lower temperatures of D_3 relative to D_2, enhancing competence contrasts which promoted buckle folding leading to space problems, and favoring reactivation of D_2 fractures and propagation of D_3-fractures and brecciation; 4) Large competence contrasts between calcite-rich and calcite-poor lithologies in the Corella Formation, with brecciation occurring in sequences with a low proportion of marbles; and 5) Inferred elevated fluid pressure and strain rate associated with pluton emplacement, most abundant in the Cloncurry District.

Widespread brecciation in the Cloncurry District allowed metasomatic fluids access to large volumes of rock, now recorded by widespread metasomatic assemblages. Regional scale alteration and its implications for Fe-oxide-Cu-Au mineralisation are the focus of **Chapters 6** and **7**.

APPENDIX 4.A

APPENDIX 4.A
CALCULATIONS FOR FIGURE 4.15

The area ratio [R] of a Class 3b fold to a Class 2 fold (A_{3b} : A_2) corresponds with the minimum amount of incompetent material required to accommodate space problems associated with Class 1b folding of competent layers within a two member (competent and incompetent) layered sequence, without appealing to accommodation structures (e.g. décollement zones, saddle reefs etc.). The above parameters can be solved for sinusoidal curves at a given amount of layer shortening, using layer thickness and initial wavelength as input parameters. Alternatively, as undertaken here, initial or wavelength can be calculated from the viscosity ratio of the competent layer to the incompetent matrix. Area calculations have been carried out for ½ wavelengths (ie. a single fold crest, from inflection point to inflection point).

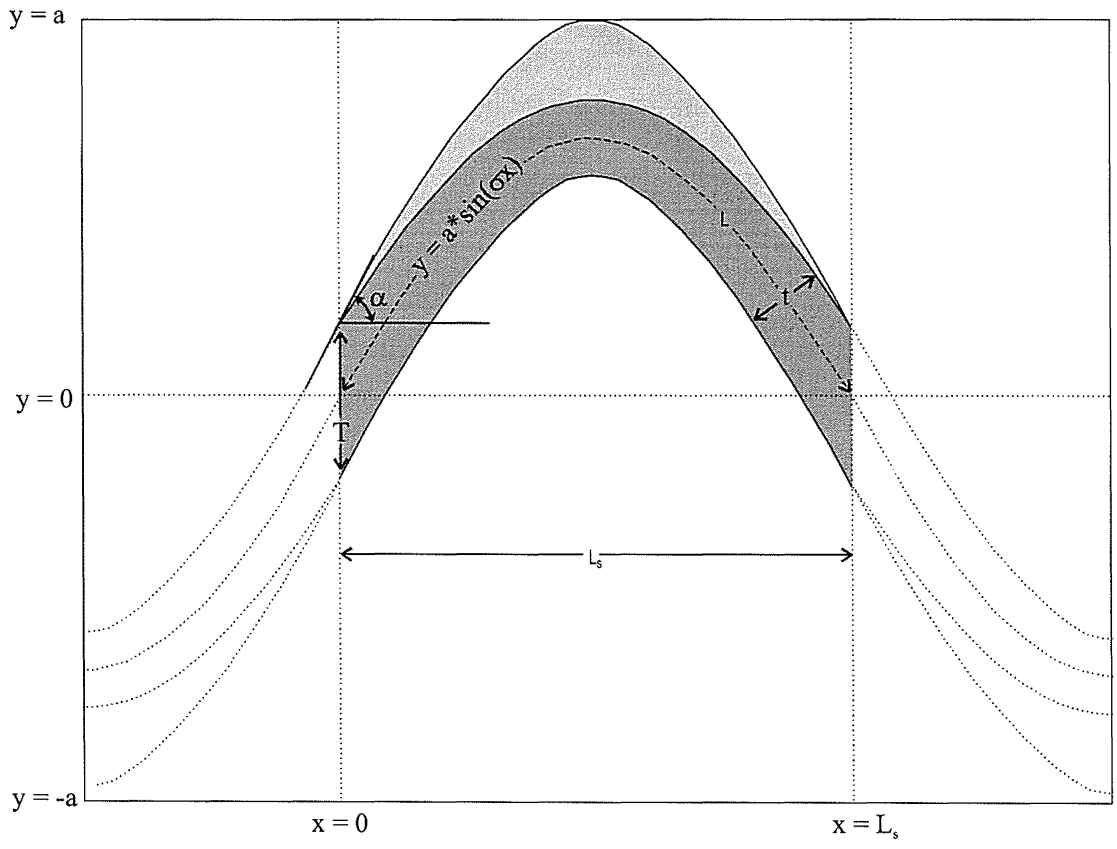

Figure 4.A.1
Illustration of geometric fold parameters.

By definition (Ramsay, 1967), Class 1b folds maintain constant area (A_{1b}) in profile section, and as such,

$$A_{1b} = t * L \quad (4.A.1)$$

Where, t = the layer thickness (input parameter)
L = initial ½ wavelength

For a competent layer embedded in an incompetent matrix, L can be estimated from the Biot (1959) – Ramberg (1959) equation,

$$L = 2\pi t (\eta_l/6\eta_m)^{1/3} \quad (4.A.2)$$

Where, η_l / η_m = layer : matrix viscosity contrast (input parameter)

The geometry of sinusoidal curves is defined by,

$$f(x) = a * \sin(\sigma x) \quad (4.A.3)$$

Where, a = fold amplitude
x = horizontal vector (relative to an upright fold train)
σ = fold frequency

In Eqn. 4.A.3, the frequency (σ) is given by

$$\sigma = 2\pi / L_S \quad (4.A.4)$$

Where, L_S = length after shortening,

L_S can be calculated from

$$L_s = L - L * (\%\text{shortening}) \quad (4.A.5)$$

Where %shortening is an input model parameter (e.g. 10, 20, 30% etc.).

The length of a sinusoidal curve (S) is given by integration,

$$S = \int_0^{Ls} (1 + f'(x))^{1/2} \quad (4.A.6)$$

Where f'(x) is given by differentiating Eqn. 4.A.3,

$$f'(x) = a * \sigma * \cos(\sigma x) \quad (4.A.7)$$

Assuming constant layer length during buckle folding,

$$S = L \quad (4.A.8)$$

Note that Eqn. 4.A.6 cannot be solved directly. However, substituting the L value from Eqn. 4.A.2 in the place of S in Eqn. 4.A.6, fold amplitude can be solved by iteration.

The slope of the sinusoidal curve is given by,

$$f'(x) = a * \sigma * \cos(\sigma x) \quad (4.A.9)$$

The fold surface dip angle (α) at the origin (x = 0) is given by,

$$\alpha_{x=0} = \tan^{-1}(f'(x = 0)) \quad (4.A.10)$$

The layer thickness parallel to the axial plane (T) is given by,

$$T = t / \cos(\alpha_{x=0}) \quad (4.A.11)$$

Given that Class 2 folds maintain constant thickness parallel to the fold's axial plane, the area of a Class 2 fold (A_2) is given by,

$$A_2 = T * L_S \quad (4.A.12)$$

By definition, the area of a Class 3b fold is given by,

$$A_{3b} = A_2 - A_{1b} \quad (4.A.13)$$

Using output from Eqns. 4.A.12 and 4.A.13, the area ratio [R] of a Class 3b fold to a Class 2 fold, and hence the minimum amount of incompetent material in a buckled sequence is given by

$$R = 100 * A_{3b}/A_2 \quad (4.A.14)$$

The minimum percentage of incompetent material has been calculated at 10, 20, 30, 40 and 50% shortening, using the following input parameters:

$t = 1$

$\eta_l / \eta_m = 1000$

Yielding the following results:

Table 4.A.1

%shortening	**10**	**20**	**30**	**40**	**50**
L_s	31.12	27.66	24.20	20.75	17.29
σ	0.20	0.23	0.26	0.30	0.36
a	3.43	4.79	5.76	6.53	7.16
$Slope_{x=0}$ ($\Delta y/\Delta x$)	0.69	1.09	1.50	1.98	2.60
$Alpha_{x=0}$ (radians)	0.61	0.83	0.98	1.10	1.20
T	1.22	1.48	0.00	2.22	2.79
A_{1b}	34.58	34.58	34.58	34.58	34.58
A_2	37.87	40.86	43.56	46.00	48.17
A_3	3.29	6.28	8.98	11.42	13.59
R (%)	**8.69**	**15.37**	**20.62**	**24.83**	**28.22**

R(%) values in Table 4.A.1 are plotted in Figure 4.15. Notably, so long as t, η_l/η_m and L are related by the Biot (1959) – Ramberg (1959) equation, calculated R(%) values are independent of the input values for t and η_l/η_m and vary only with fold shape (here calculated for sinusoidal Class 1b folds).

EXAMPLES OF DILATIONAL FAULT ZONE BRECCIATION AND VEINING IN THE EASTERN SUCCESSION, MT ISA BLOCK, AND DISCUSSION OF POTENTIAL GENETIC MECHANISMS

EXAMPLES OF DILATIONAL FAULT ZONE BRECCIATION AND VEINING IN THE EASTERN SUCCESSION, MT ISA BLOCK, AND DISCUSSION OF POTENTIAL GENETIC MECHANISMS

5.1 INTRODUCTION

Breccias and associated veins have long been recognized as important ore hosts for a wide variety of mineralisation styles (e.g. Spurr, 1925; Hulin, 1929; Phillips, 1972; Sillitoe, 1985). In addition to providing physical sites for ore deposition, these structures provide high permeability conduits that can serve to focus metasomatic fluid flow. Breccias and veins formed at dilational jogs in faults and shear zones have been shown to be particularly effective in localizing ore deposits, or high grade mineralisation within deposits. Examples include high grade-gold mineralisation in the Roamane fault, Porgera gold mine, Papua New Guinea (Corbett et al., 1995), the Ashanti deposit in Ghana (Allibone et al., 2002) and numerous examples from the Lachlan Fold Belt, Australia (e.g. Cox, 1995; Schaubs and Wilson, 2002).

In this chapter, various occurrences of brecciation and veining associated with dilational fault jogs and flexures are documented, with descriptions drawn from both economically barren and mineralised systems in the Eastern Succession of the Mt Isa Block, Australia (Fig. 5.1). Variations in brecciation and veining style can in part be attributed to fault mode (i.e. reverse, strike-slip or normal) and the permeability of rocks surrounding the fault zone. This contribution builds on the previous work of Oliver et al. (1990) and Davis (1997) in the Eastern Succession. While these authors addressed issues including the channeling of metasomatic fluid flow into a variety of structural conduits, controls on variations in brecciation and veining style within dilational fault zones have not previously been widely addressed in the Eastern Succession. Here likely controls on the genesis of implosion breccias, large width veins (>1m width), forced magmatic-hydrothermal breccias and fluidized and gas stream breccias formed within dilational fault zones are considered.

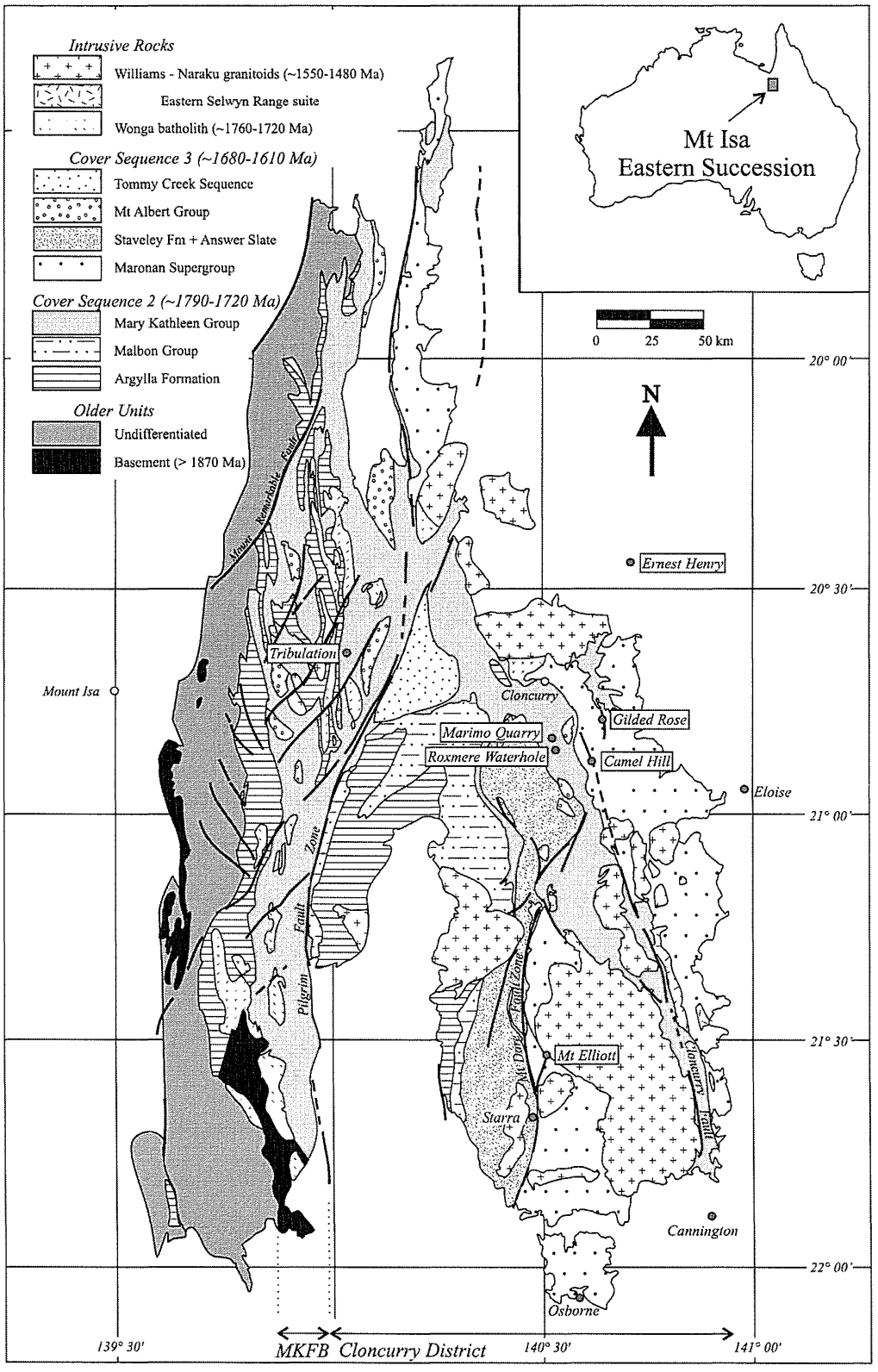

FIGURE 5.1.
Simplified geology of the Eastern Succession, Mt Isa Inlier. Modified after Williams (1998).

5.1.1 Dilational fault zones and brecciation

Zones of dilation commonly result from slip along faults or shear zones with favorably oriented irregularities or jogs. Such irregularities are commonly the result of pre-existing intersecting structures, or the intersection of fault zones with rocks of varying competence. In the simplest case, a step-like jog along a planar fault zone will result in a near linear to tabular zone of dilation lying within the fault plane and orthogonal to the slip vector (Fig. 5.2). Dilation commonly results in increased permeability, evidence for which may be preserved by minerals precipitated as infill in interconnected veins and/or breccias. For the purposes of this chapter, dilational zones are defined as regions within faults that preserve such interconnected veins and breccias. Within these zones, increased fluid connectivity may allow for the attainment of near hydrostatic fluid pressure gradients (although not necessarily at hydrostatic values) during and immediately following fault slip (Fig 5.2). This scenario is analogous to an enclosed cylinder of water, within which there is a hydrostatic fluid pressure *gradient*, even if the cylinder is pressurized resulting in suprahydrostatic fluid pressure *values*.

Sibson (1986) notes that the fundamental concepts related to dilational fault jogs are equally applicable to all modes of faulting. That is, dilational zones with similar shapes are expected to form regardless of the fault mode (i.e. reverse, strike-slip or normal). However, the orientation of dilational zones will vary depending on the fault mode, with the long axis of dilational zones being near vertical in strike-slip faults, and near horizontal in normal and reverse faults (Fig. 5.2). Fault mode and its influence on the vertical continuity of dilational zones will impart a critical control on local fluid pressure gradients. This in turn may affect the character of associated breccias and veins, and their suitability as ore hosts. Fault mode is primarily a function of the stress regime, which may vary significantly within a regional tectonic setting due to crustal heterogeneity.

Wallrock permeability will affect the rate at which fluid pressure gradients stabilize following fault slip, and as such provides an additional control on resultant veining and brecciation style. Thus in long-lived fault-systems, breccia and vein character may vary with time, in response to changes in permeability.

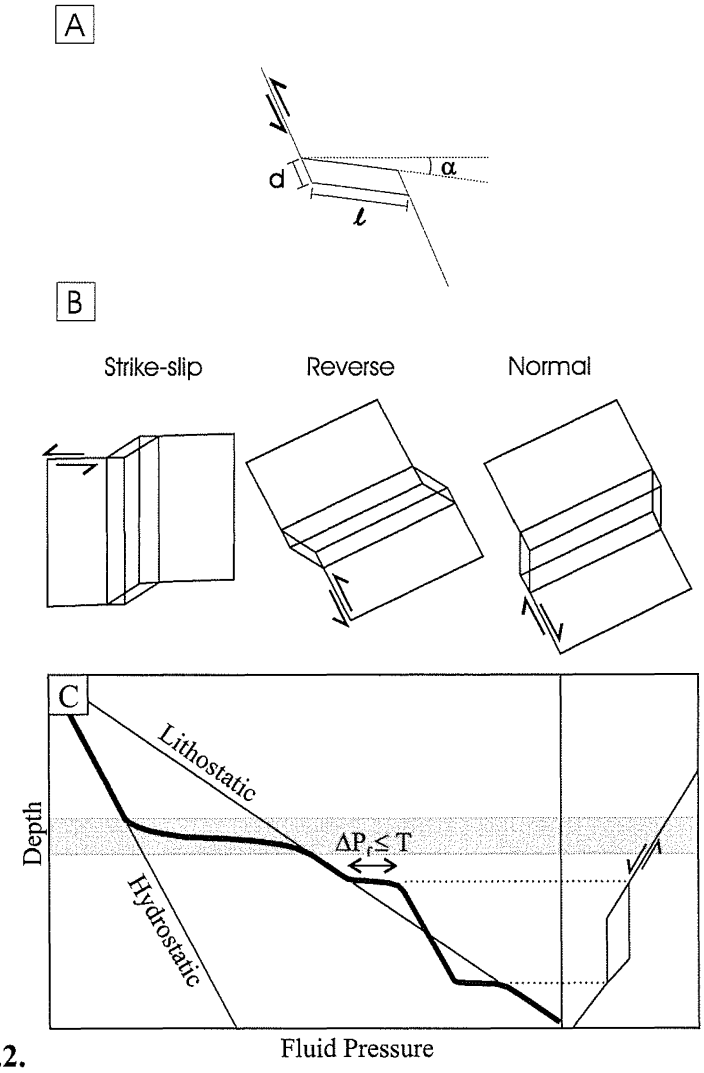

FIGURE 5.2.
(a) Illustration of variables constraining the geometry of dilational jogs, shown here for a reverse fault. L = length of jog, d = magnitude of displacement, a = dip of jog. (b) Strike-slip faults contain dilational zones with a near vertical long axis, while normal and reverse faults contain near horizontal dilational zones. Where the length of a dilational jog is greater than the magnitude of displacement (pictured), the intermediate axis of the dilational zone will be near vertical for normal faults and near horizontal for strike-slip and reverse faults. Modified after Cox et al. (2001). (c) Influence of vertical continuity of dilational zones on the magnitude of shifts in fluid pressure gradients surrounding the dilational zone (ΔPf), shown here for a schematic normal fault. Fluid pressures have been shown to be at near hydrostatic values in the shallow crust where interconnected fluid-filled fractures are present, and at near-lithostatic values at depth, below low permeability seals (shaded region in schematic diagram). The bold solid line in Fig 5.2c represents a theoretical fluid pressure curve. Within dilational zones, fluid pressure will strive to achieve a hydrostatic gradient (as for a column of water), albeit at near lithostatic pressure values, resulting in overpressuring at the top of the dilational zone, and underpressuring at the base of the dilational zone, relative to the surrounding rocks. Maximum values of ΔPf are limited by the tensile strength of surrounding rocks.

Here, breccias are treated as being composed of three components: clasts, matrix and infill (Taylor and Pollard, 1993), and are described using the qualitative terms crackle, mosaic, rubble and milled. These terms are defined in **Chapter 4** (section 4.1.1).

5.1.2 Regional geology

Examples in this chapter are drawn from the Mary Kathleen Fold Belt and Cloncurry District of the Eastern Succession, Mt Isa Block, Australia (Fig 5.1). The Mary Kathleen Fold Belt (MKFB) is dominated by scapolitic calc-silicate rocks, metasiltstones, and mafic and felsic meta-volcanic rocks of the Mary Kathleen Group (ca. 1790 to 1720 Ma). These rocks were intruded by mafic and felsic intrusives of the Wonga suite during an early extensional episode (ca. 1760 to 1720 Ma). Intense deformation (D_2 and D_3 regionally; Oliver et al., 1991) accompanied amphibolite facies peak metamorphism (ca. 1575 Ma; Hand and Rubatto, 2002) and retrograde metamorphism, and involved the formation of upright north-trending folds, and pervasive axial planar fabrics. Syn- to post-peak metamorphic brecciation and veining was largely focussed along brittle-ductile to brittle fault zones, and along contacts between Corella Formation metasedimentary rocks and relatively competent pre-metamorphic Wonga intrusions and associated skarns (Oliver and Wall, 1987; Oliver et al., 1990). Vein and breccia formation was accompanied by intense Na-(Ca) metasomatism.

The Cloncurry District (Fig. 5.1) is dominated by three main rock sequences, including Mary Kathleen Group marbles and calc-silicate rocks, younger siliciclastic metasediments and mafic volcanics of the Maronan Supergroup, including the Soldiers Cap Group (ca. 1680 - 1620 Ma), and granitoids of the Williams and Naraku batholiths (ca. 1550 - 1500 Ma). Peak metamorphic conditions reached upper greenschist to amphibolite facies (ca. 1600 - 1584 Ma; Page and Sun, 1998; Giles and Nutman, 2002). While brecciation is locally well developed in the Maronan Supergroup (e.g. de Jong and Williams, 1995), breccias are most widespread in the Corella Formation, and include the Corella and Gilded Rose Breccias. The Corella breccias are in part a result of heterogeneous folding of marble

and calc-silicate rock sequences that were fractured and boudinaged in part during earlier deformation events (**Chapter 4**, this study). In many places, the Corella breccias acted as conduits for significant fluxes of metasomatic fluid at moderate to high temperatures (ca. 350 to >500°C; de Jong and Williams, 1995). Gilded Rose breccias are distinguished from the Corella breccias by evidence for significant clast transport and clast mixing. The depth of brecciation is poorly constrained, but the Corella breccias show mixed brittle-ductile characteristics and commonly record Na-(Ca) rich alteration assemblages similar to those documented by de Jong and Williams (1995) at pressures of ca. 200MPa. (i.e. ca. 7-8 km depth). The Gilded Rose breccias record purely brittle characteristics and associated intrusions exhibit features including miarolitic cavities and porphyritic textures that are typical of epizonal environments. These features may indicate partial exhumation synchronous with brecciation.

A well-developed fault array throughout the Eastern Succession (Fig. 5.1) was active during D_3 and broadly synchronous post-peak metamorphic intrusion and metasomatism. All examples described in this contribution are associated with fault slip attributed to D_3, although absolute timing of each slip event is poorly constrained. For the most part, the fault array shows apparent lateral offset on conjugate faults which suggests late fault movement in response to predominantly east-west directed shortening (e.g. Laing, 1998), although local deviations in shortening direction are noted.

O'Dea et al. (1997) proposed that D_3 records a transition from compressional to wrench (i.e. transtensional) tectonics during the waning phases of the Isan Orogeny. Late- and post-D_3 deformation was increasingly accommodated by strike-slip deformation along major interconnected fault zones. Further, the dominant NNE to NNW strike and moderate to steep dip of late faults in the Eastern Succession is inconsistent with forming in response to E-W directed shortening. As such, the average fault orientation likely reflects either reactivation and/or rotation of earlier structures, localization of late faults in regions of crustal weakness, or a change in compression direction late in the tectonic history of the area.

5.2 FIELD EXAMPLES OF DILATIONAL FAULT ZONES

5.2.1 Mt Elliott Cu-Au

Mt Elliott is a small but relatively high-grade Cu-Au deposit (2.9 Mt @ 3.33% Cu and 1.47 g/t Au; Fortowski and McCracken, 1998) located in the southern Cloncurry District (Fig. 5.1). The deposit formed in the waning phases of the Isan Orogeny, and is hosted by an intensely altered and deformed sequence of schist, phyllite and amphibolite of the Kuridala Formation, and is characterized by skarn-like mineral assemblages.

Little (1997) outlined a protracted deformation and alteration history at the deposit. Mineralisation is localized by Jocks fault, a comparatively shallow-dipping fault which links the more steeply dipping Footwall fault and a zone of localized shearing termed the Hangingwall shear (Fig. 5.3). Asymmetrically boudinaged quartz veins within the Footwall fault were interpreted by Little (1997) to record predominantly reverse movement. The development of pre- and syn-mineralisation milled breccias is broadly confined to a zone along the Footwall fault. While some mineralisation is hosted in milled breccias, the bulk of mineralisation occurs in adjacent zones of crackle breccias, along and above Jocks Fault.

Upper zone mineralisation (Fig. 5.3) forms the upper portion of the outer caparace breccia and occurs predominantly as infill in a network of centimetre-scale fractures. This extensively developed crackle breccia lacks a significant matrix component and exhibits minor block rotation. Little (1997) suggested that this zone may represent the upward termination of the Hangingwall shear. The outer carapace breccia grades downwards towards Jocks Fault into Lower zone mineralisation characterized by metre-scale dilational vugs between angular to subangular rotated breccia blocks, as well as sheet-like extensional veins which mirror the orientation of Jocks Fault (Fig. 5.3). Dilational openings typically exceed 10cm in width, reach up to 7m in thickness and extend up to 60m down-dip (Little, 1997). The shallow dip to these extensional gashes is consistent with forming in a transfer zone between the Footwall fault and Hangingwall shear during predominantly reverse slip on these structures. Infill mineralogy is characterized by a skarn-like assemblage of magnetite + pyrite + chalcopyrite + pyrrhotite + calcite ± garnet, actinolite, titanite,

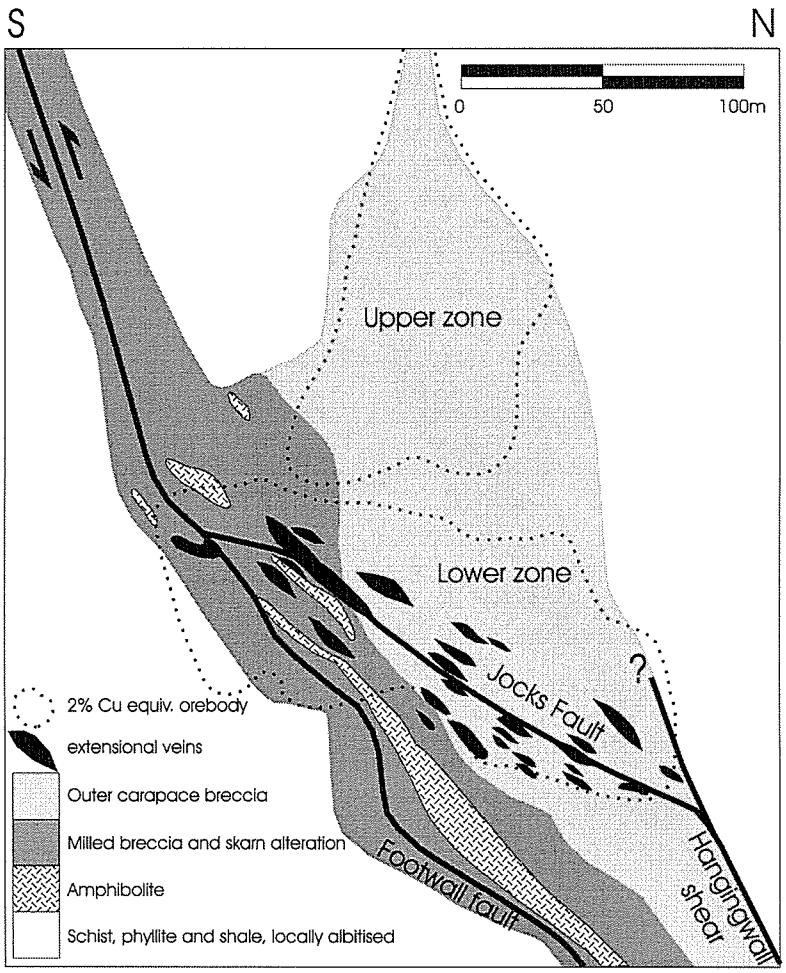

FIGURE 5.3.
Simplified N-S cross section through the Mt Elliott Cu-Au deposit. Kinematic indicators along the Footwall fault indicate predominantly reverse movement. Modified from Little (1997).

epidote, biotite, hematite, albite, K-feldspar and chlorite and late gypsum. Some vugs remained open after mineralisation, perhaps suggesting a relatively shallow depth of ore formation. Ore minerals occur primarily as infill, and are locally extremely coarse-grained (grains commonly 5-100cm) (Fig. 5.4). Little (1997) inferred from stable isotope data that ore fluids were magmatic, and mineral precipitation occurred at temperatures between approximately 350° and 500°C. Based on a lack of overprinting features, the outer carapace breccia has been interpreted as the result of only one tectonic event (Little, 1997).

Key characteristics of the Mt Elliott deposit include its setting at a dilational jog in a reverse fault, and extensive crackle breccias characterized by coarse-grained infill. Mineralisation occurs predominantly within large extensional veins and large vugs between angular clasts that exhibit minor rotation and transport.

5.2.2 Roxmere-Marimo shear zone

Outcrops at the Roxmere waterhole and the Marimo quarry occur within a brittle-ductile shear zone developed within shallowly north-dipping meta-siltstones and subordinate calc-silicate rocks of the Corella Formation in the Cloncurry District (Fig. 5.1). Shear-related deformation occurred post-peak upper greenschist facies metamorphism and tight to isoclinal folding (ca. 1600-1570 Ma), and possibly synchronous with similar deformation and metasomatism in the Mary Kathleen Fold Belt at ca. 1530-1525 Ma (Oliver et al., in revision; see also Tribulation section below).

An approximately 1km wide NNW-trending zone of intense veining and brecciation characterizes the Roxmere-Marimo shear zone. A well-developed interconnected fracture and breccia network strikes predominantly to the NNW with an overall near-vertical dip and with consistent apparent sinistral offset across fractures (Fig. 5.5). Mesoscopic fractures are poorly developed in calcite-rich calc-silicate rock horizons. Locally however, calc-silicate rock layers cross-cut bedding in adjacent meta-siltstones (Fig. 5.5b), recording a significant component of plastic flow.

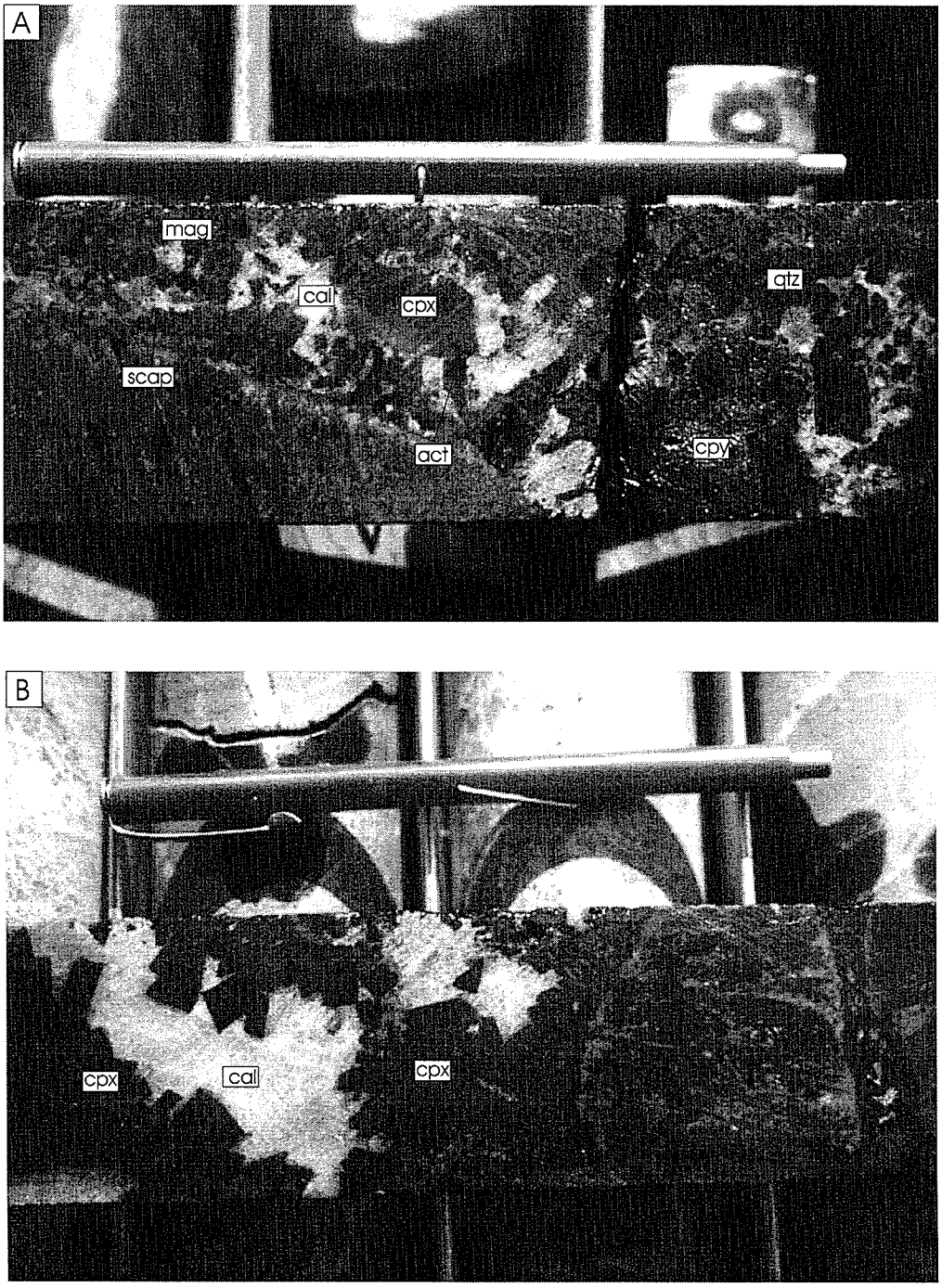

FIGURE 5.4.
Mt Elliott Outer carapace breccias, with coarse-grained calcite + actinolite, diopside, scapolite, magnetite and sulfide infill between blocky clasts (pen magnet = 12cm).

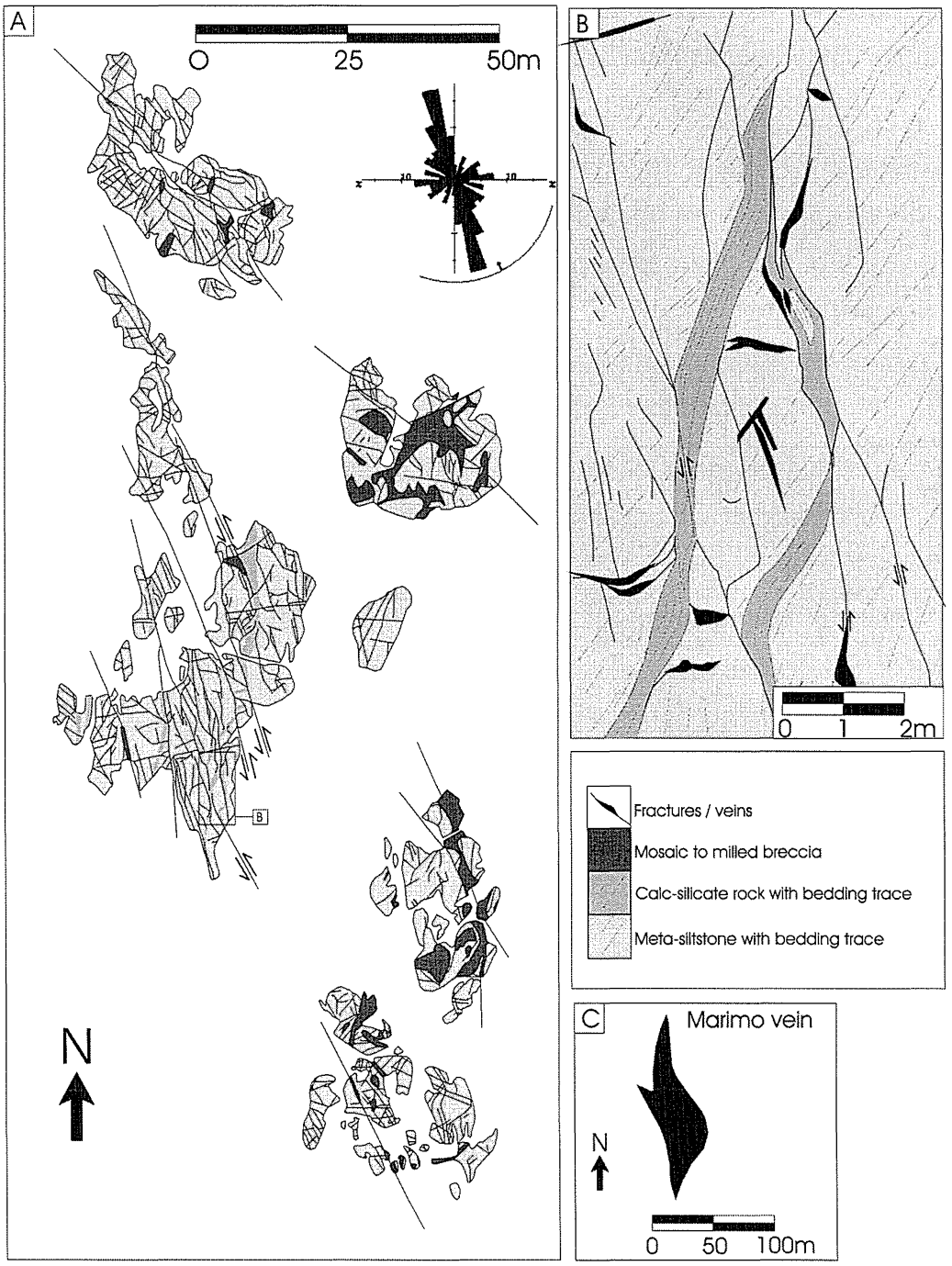

FIGURE 5.5.
(a) Outcrop map from the Roxmere waterhole. Interconnected fractures and breccias define an anastamosing shear zone, with consistent apparent sinistral displacement. Rose diagram illustrates the predominant NNW fracture trend. (b) Enlargement of area indicated in Fig. 5.5a. Strain within calc-silicate rock layers is predominantly accommodated by ductile shearing, while more competent siltstones are more prone to through-going brittle fracture. (c) The calcite-dominated Marimo vein, 2.4km to the NNW, strikes approximately 340° with a near vertical dip. The vein has a minimum vertical extent of 40m. The geometry of the vein is consistent with forming during sinistral strike-slip displacement.

Breccias are common within the Roxmere-Marimo shear zone and grade from local crackle breccias to progressively more milled breccias with a high matrix component and relatively small infill component (Fig. 5.6). Locally the breccias exhibit a moderately well developed matrix fabric, characterized by the alignment of breccia clasts and matrix minerals (Fig. 5.6). The breccias are intensely altered to albite + actinolite ± diopside, magnetite, apatite and calcite assemblages and are interconnected with veins of similar mineralogy.

Actinolite-rich breccias and veins are consistently cut by calcite-dominated extensional veins, including the large Marimo vein (Fig. 5.6). The latter are characterized by predominantly fine-grained (<1cm) calcite grains, with subordinate actinolite, quartz, biotite, magnetite, pyrite, chalcopyrite and molybdenite. The calcite-rich veins are all steeply dipping, and strike between approximately 270 and 340°, commonly as dilational linking jogs between NNE-trending shear fractures. Some of the veins, including the Marimo vein, are metres to tens of metres in thickness. Local inclusions of coarser-grained infill (5-10 cm) are preserved, suggesting that the veins may originally have been coarse grained, and have subsequently been recrystallized. Some wallrock clasts are found within the larger veins.

Key characteristics of the Roxmere-Marimo shear zone include apparent strike-slip deformation across a broad (ca. 1km wide) shear zone, early widespread fracture and breccia networks, and late, large width calcite-rich veins containing some wallrock clasts.

5.2.3 Tribulation calcite vein

The Tribulation and Lime Creek veins lie within meta-siltstones, calc-silicate rocks, marbles, schists and metadolerites of the lower Corella and Argylla Formations in the Mary Kathleen Fold Belt (Figs. 5.1 and 5.7). The veins likely formed synchronous with similar veining and metasomatism at the nearby Knobby quarry at ca. 1530-1525 Ma (Oliver et al., in revision).

Both the Tribulation and Lime Creek veins lie along the NNW-trending Tribulation – Lime Creek (TLC) fault, which cuts and offsets D_2 folds. The lack of

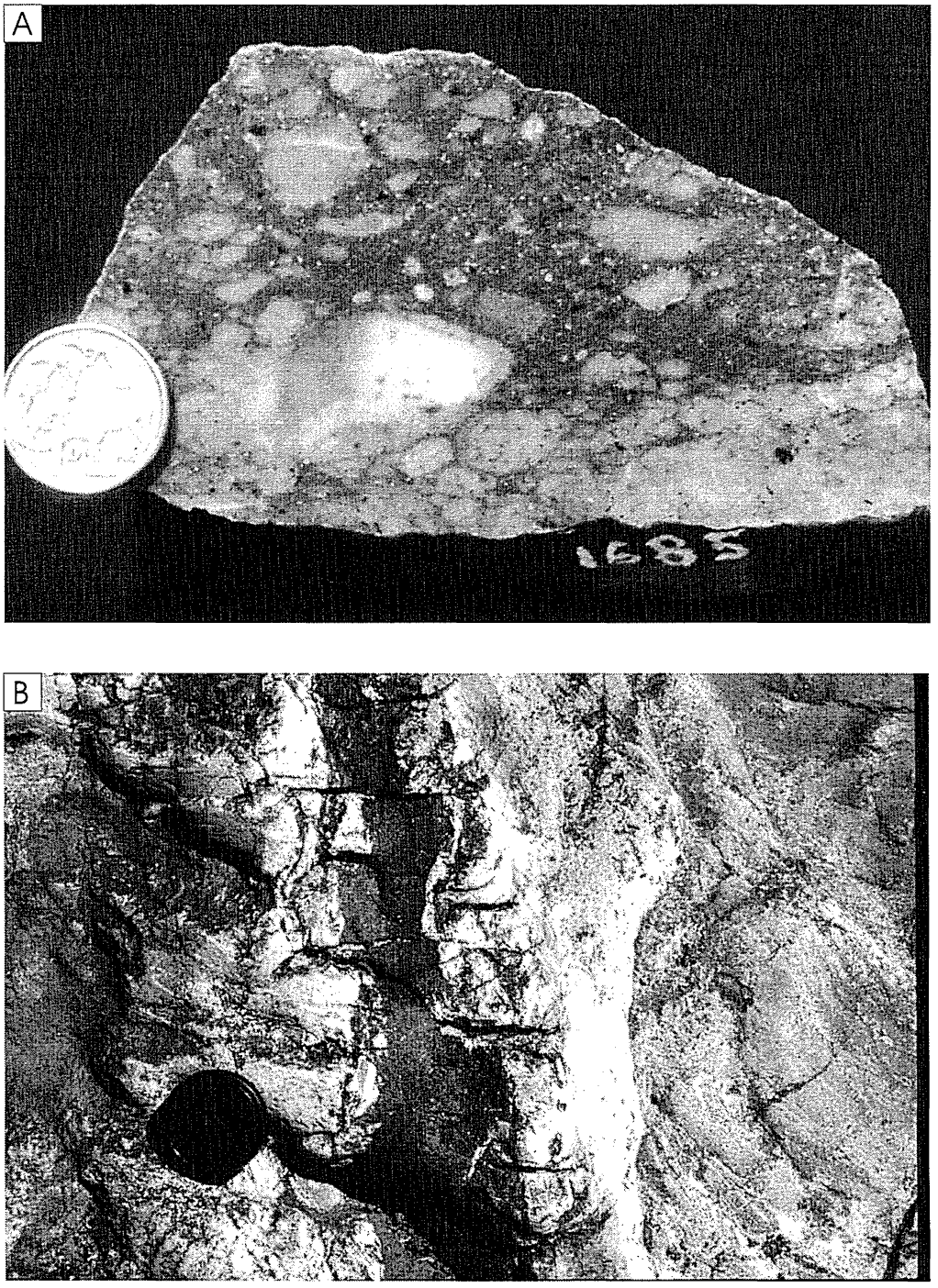

FIGURE 5.6.
(a) Milled, matrix supported breccia with moderate matrix fabric, from near the Marimo Quarry (coin = 2.4cm diameter). (b) NNW-trending actinolitic shear vein cut by E-W trending calcite-rich extensional veins at the Roxmere waterhole (lens cap = 5cm diameter). Note bleaching of wallrocks adjacent to the vein as a result of albitisation. North is to the top of the photo.

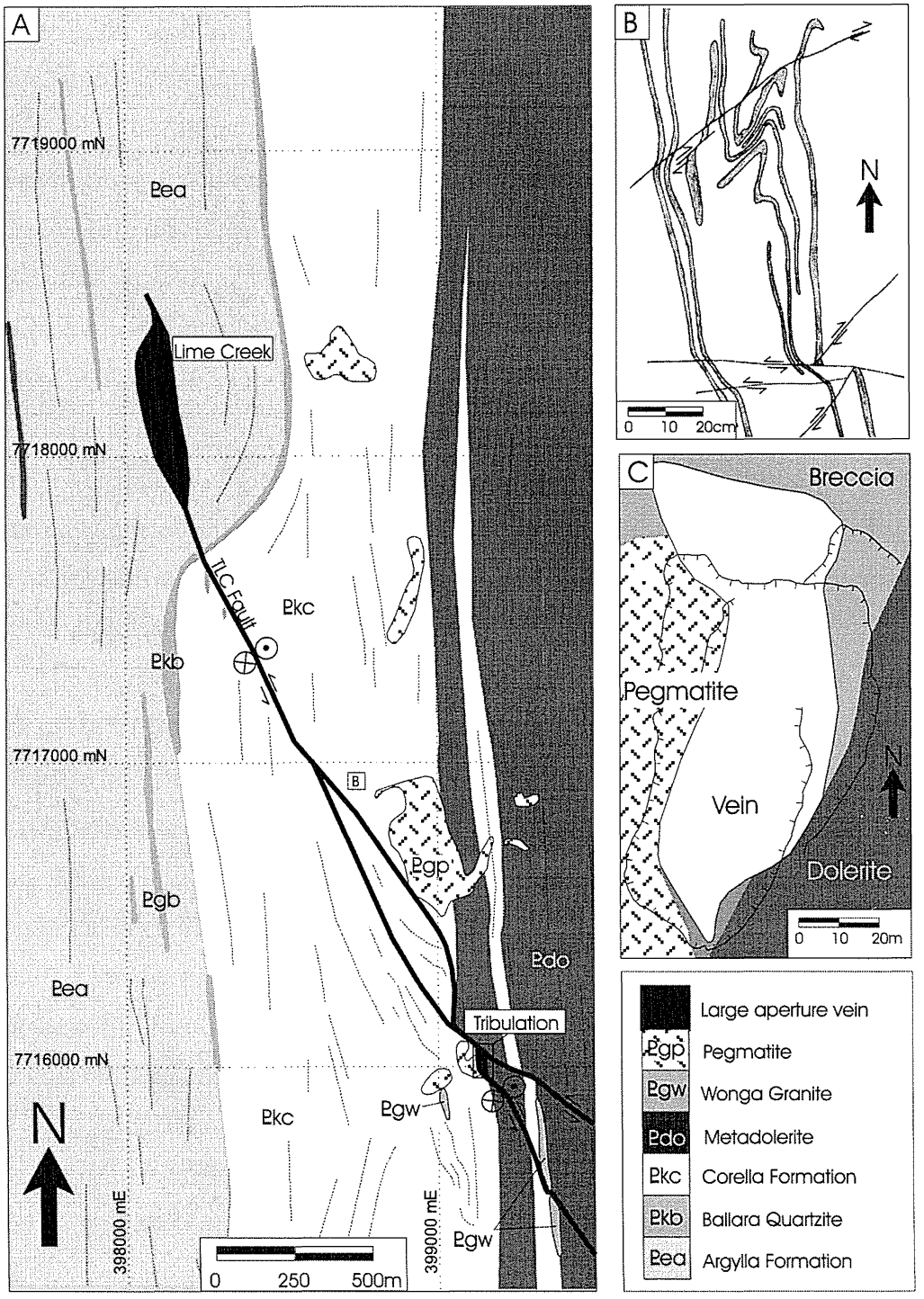

FIGURE 5.7.

(a) Geologic map of the Tribulation - Lime Creek area. (b) Sketch from an outcrop photograph of D_2 folds and fold limb boudins in calc-silicate (grey) and marble (white) stratigraphy, illustrating mutually cross-cutting conjugate D_3 fracture set consistent with ENE-WSW directed shortening. (c) Sketch map of the geometry of the Tribulation vein. Quarry pit walls are also indicated. The main portion of the vein dips shallowly to the east, while the western margin of the vein bends upwards into a steeply east-dipping orientation, matching the inferred orientation of the TLC fault. The northern and southern ends of the vein taper out within breccia zones.

deflection of the fault trace across topographic features suggests a steep dip to the fault plane. Zones of milled breccias are found along the TLC fault, and adjacent to the pegmatites. Locally, the breccias contain clasts of pegmatite, and are cut by dykes of pegmatite, confirming that periods of brecciation and intrusion overlapped. The breccias are mainly composed of clasts of Corella Formation calc-silicate rocks and metadolerite, with both clasts and matrix being intensely altered to albite + actinolite ± diopside, biotite, titanite and apatite. The breccias are clast- to matrix-supported and contain a low proportion of infill (Fig. 5.8). The large width Tribulation and Lime Creek calcite-dominated veins cut the breccias, and are not themselves brecciated. Breccia-vein contacts are sharp but locally irregular, with vein terminations exhibiting several branches. Lime Creek is the larger of the two vein systems, but it is variably recrystallised (typical grain size 1-30cm) and contact relationships are poorly exposed compared with the Tribulation vein.

The exposed portion of the Tribulation vein lies at the junction of two strands of the TLC fault, and at the contact between a N-S trending, sub-vertical metadolerite body to the east, and Corella Formation calc-silicate rocks intruded by a post-D_2 pegmatite body to the west (Fig. 5.7). The upper and most westerly portion of the vein dips steeply to the east, and curves down-dip into the main section of the vein, which dips shallowly to the east. This east-dipping sigmoidal geometry is most consistent with forming at a shallow east dipping dilational jog within the more steeply dipping, reverse TLC fault. The basal contact to the Lime Creek vein also dips shallowly to moderately to the ESE.

The Tribulation vein is extremely coarse-grained with calcite crystals in excess of $1m^3$, actinolite crystals over 1m in length, and apatite, titanite, biotite and diopside grains approaching 20cm across (Fig. 5.8). Rare magnetite (<5mm) is also noted. A consistent mineral zonation exists within Tribulation and other similar veins in the MKFB: apatite, titanite, biotite, quartz and diopside grains are found immediately adjacent to the vein margins, splays of actinolite crystals radiate inwards from these, and the cores of the veins are dominated by calcite. The preservation of coarse grain sizes and the sharp vein-breccia contacts suggests that veining occurred late- to post-brecciation.

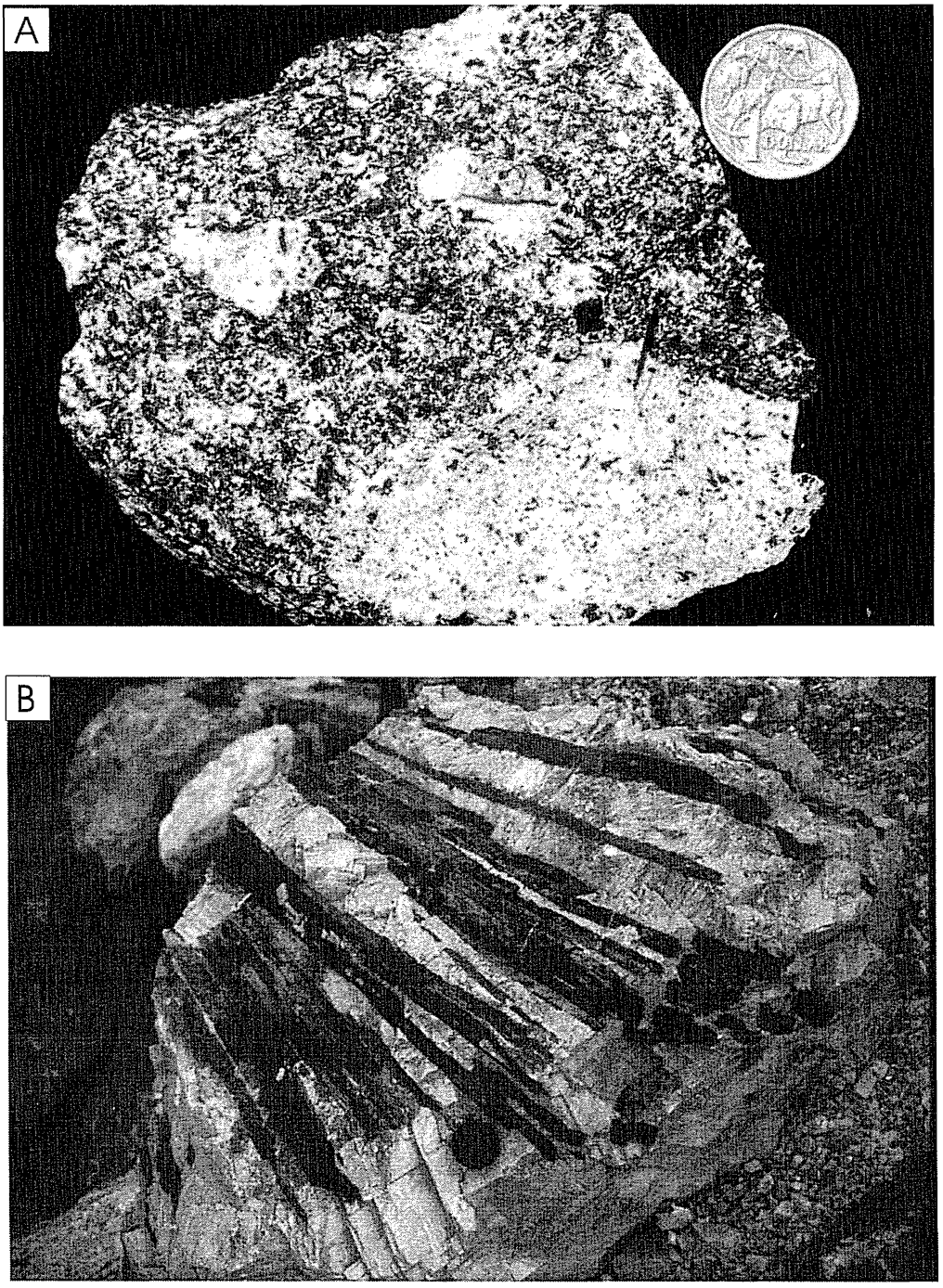

FIGURE 5.8.
(a) Milled matrix supported breccia from the Tribulation quarry. Coin = 2.4cm diameter. (b) Extremely coarse-grained actinolite and calcite infill from the Tribulation vein. Lens cap (bottom center) = 5cm diameter.

Key characteristics of the Tribulation vein include its occurrence at the dilational intersection between the steeply-dipping TLC fault and a near-vertical dolerite body, early milled breccias, and the extremely coarse, intergrown and euhedral nature of all grains in the vein.

5.2.4 Gilded Rose breccia type area

Gilded Rose breccias crop out over tens of square kilometres in the Cloncurry District, both within Corella Formation rocks, and as discrete bodies that have seemingly intruded Soldiers Cap group rocks. The type area lies within several kilometres of Gilded Rose mine, and all Gilded Rose references herein refer to the breccias and not the mine. The Gilded Rose breccias post-date all folding episodes, and a K-Ar muscovite age of 1488 ± 11 Ma from the breccia type area has been interpreted as a minimum age for some of the breccias (Perkins and Wyborn, 1998).

Although a fault association is not always apparent (or necessarily required) the Gilded Rose breccias were commonly emplaced at dilational jogs in steeply-dipping strike-slip faults (Fig. 5.9). At the type area, neither fault-related foliations nor drag folds in the surrounding rocks are noted. Regional mapping combined with interpretation of seismic and aeromagnetic data (Macready et al., 1998) confirm that Corella Formation rocks underlie all occurrences of Gilded Rose breccias. For example, at Camel Hill, Gilded Rose breccias intrude Soldiers Cap group rocks that are underlain by the Corella Formation at a depth of at least several kilometres. In all cases, including at Camel Hill and the type area, Gilded Rose breccias contain a predominance of clasts derived from the Corella Formation. Given the 3D architecture of the area, with all occurrences of Gilded Rose breccias underlain at variable depths by the Corella Formation, the occurrence of Corella Formation clasts in the breccias is best explained by upward clast transport at scales of up to hundreds of metres to kilometres.

At the type area, the breccia body can be divided into an irregular NW-trending splay, and an elliptical, N-trending main body (Fig. 5.9). The NW-trending splay is characterized by milled breccias with a low component of infill, and pervasive albite + actinolite alteration, similar to milled breccias documented at

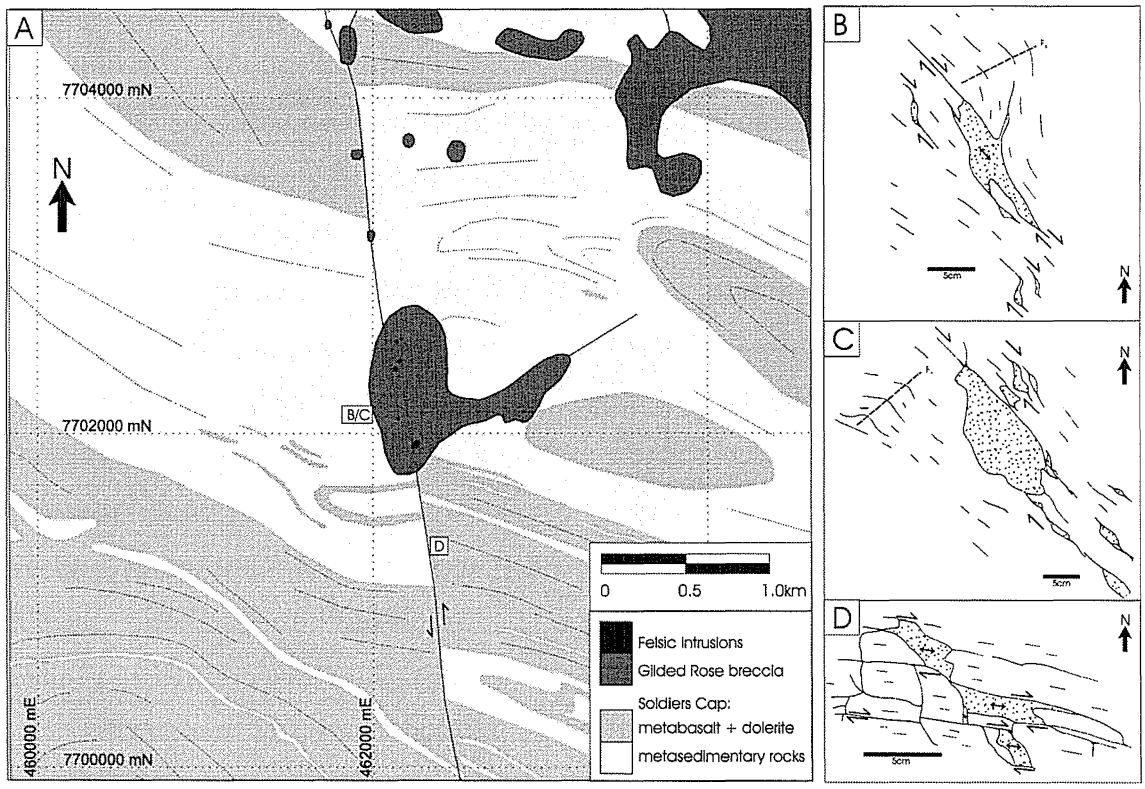

FIGURE 5.9.
(a) Geological map of the Gilded Rose breccia type area. The main breccia body is coincident with a dilational jog in a steeply-dipping, N-S trending fault. (b-d) Sketches from outcrop photographs of dilational breccias and veins (stippled) developed in Soldier's Cap group stratigraphy adjacent to the Gilded Rose fault. All sketches are in map view, with North to the top of the page. Apparent offset is consistent with SSE-NNW directed D_3 shortening. All dilational zones are steeply plunging.

Tribulation and the Roxmere-Marimo areas. The main breccia body and other occurrences of Gilded Rose breccias throughout the Cloncurry District are polymict, and at all localities contain a majority of clasts derived from the Corella Formation and Corella breccias. The breccias also commonly contain inclusions of felsic intrusions, even in regions where post-peak metamorphic intrusions are not found in the surrounding rocks (Fig. 5.9). The margins to these granitoids are often fractured and altered, with clasts being incorporated into the breccias. The intrusions exhibit a variety of distinct textures including coarse-grained spherulitic quartz-feldspar intergrowths, miarolitic cavities, and porphyritic textures (Fig. 5.10). Where the breccias are emplaced within Soldiers Cap Group rocks, clasts of these are also present, most commonly near the breccia margins.

Clasts range from subordinate angular shapes, to dominantly rounded morphologies, and range in size up to 30m or more. A matrix component is invariably present, and can range up to 70 percent of the breccia volume. An infill component ranges up to 20 percent of the breccia. The breccias show locally intensely developed early Na-(Ca) rich (albite + actinolite ± calcite ± quartz ± magnetite) infill and alteration assemblages, which pre-date the main brecciation event. A phase of K-Fe, or "red-rock" (calcite + hematite ± quartz ± biotite ± K-feldspar ± chlorite) infill and alteration of breccia matrix and clasts accompanies the main brecciation event.

Key characteristics of the Gilded Rose breccias include the spatial association with felsic intrusions and dilational jogs in predominantly strike-slip faults and extreme mixing, milling and upward clast transport.

5.2.5 Ernest Henry Cu-Au

Ernest Henry, the largest Cu-Au deposit in the Eastern Succession (166Mt @ 1.1% Cu and 0.55ppm Au; Ryan, 1998), is located 35 km northeast of Cloncurry. The deposit is predominantly hosted by Mount Fort Constantine (MFC) felsic metavolcanic rocks. Timing of mineralisation is constrained to greater than 1510 Ma (Twyerould, 1997; Perkins and Wyborn, 1998).

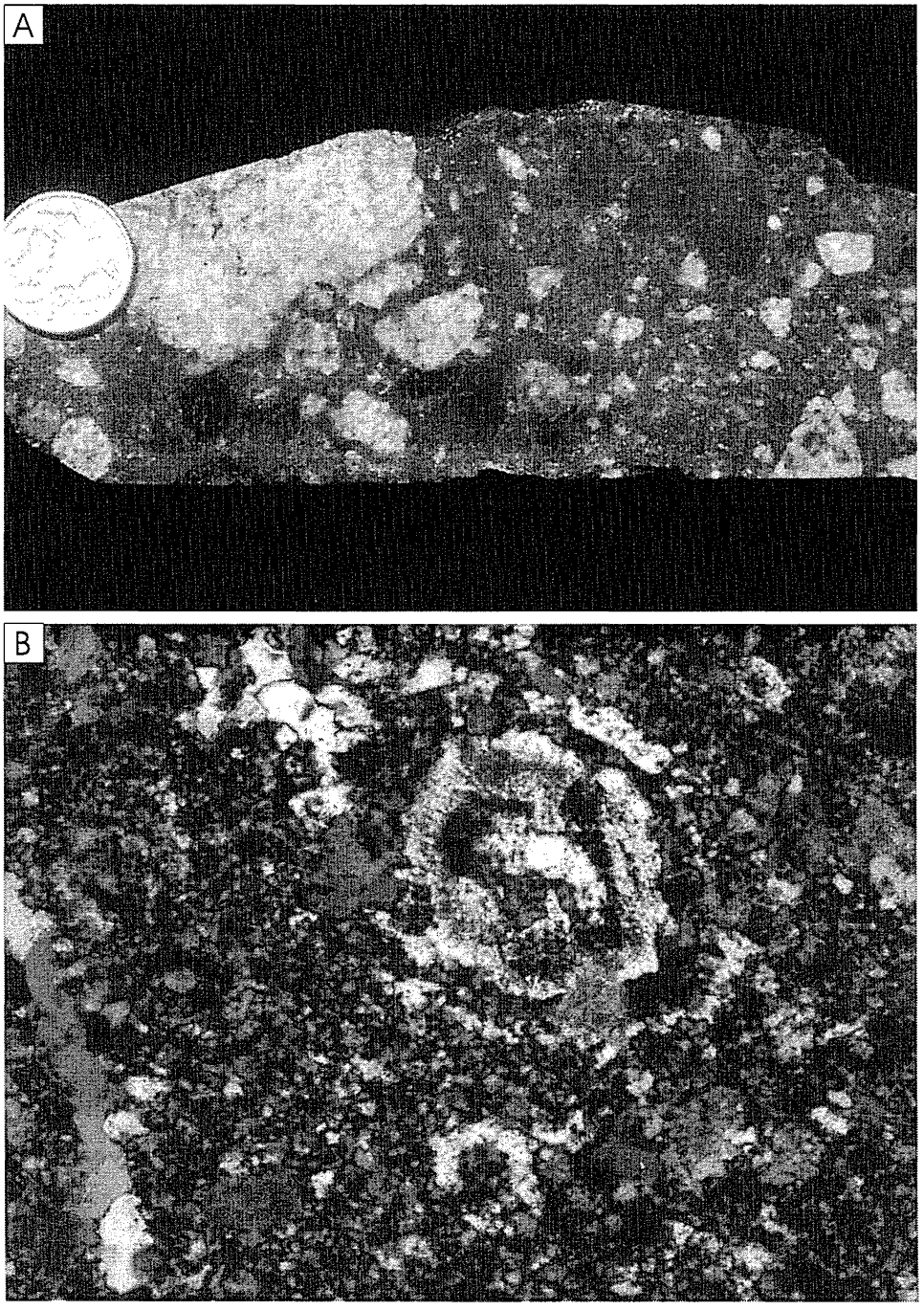

FIGURE 5.10.
(a) Polymictic, milled, matrix supported Gilded Rose breccia, with granitic and calc-silicate rock clasts (white and grey respectively; coin = 2.4cm diameter). (b) Photomicrograph (crossed polars) of spherulitic quartz-feldspar intergrowths from a granitoid within Gilded Rose breccia (width of photomicrograph = 1.4mm).

The deposit forms a pipe-like breccia body plunging approximately 45° to the SSE (Fig. 5.11). The main ore breccia grades upwards into the hangingwall through a narrow zone of clast-supported mosaic breccia into crackle brecciated volcanic rocks, and then upwards into the Hangingwall Shear Zone (HWSZ), an approximately 100m thick zone of heterogeneous shearing (Coward, 2001). Within the HWSZ, monomict milled breccias with a high matrix component (10-40%) are locally present. The main ore breccia grades downwards through a zone of variably brecciated and intensely sheared intercalated metavolcanic and metasedimentary rocks comprising the Footwall Shear Zone (FWSZ).

Much of the FWSZ consists of a medium- to coarse-grained calcite-dominated unit termed 'marble matrix breccia,' characterized by a well-developed shear fabric defined by the alignment of actinolite ± biotite, magnetite and sulphide grains (Fig. 5.12). This fabric strongly anastamoses around clasts of felsic volcanic rocks contained within the marble matrix breccia. Field observations in the Corella Formation throughout the Cloncurry District reveal very common boudinage of quartzo-feldspathic rich calc-silicate metasedimentary layers embedded within marbles. These rocks are characterized by extreme ductility in the marble horizons, with marble interpreted to have flowed into inter-boudin gaps, and elsewhere inter-boudin gaps filled with calcite-dominated infill that is texturally continuous with adjacent marble horizons. Where intensely sheared, Corella Formation marbles give rise to identical textures to those seen in the marble matrix breccia at Ernest Henry (Fig. 5.12). These observations strongly suggest that the marble matrix breccia is in fact a marble, *sensu stricto* (i.e. metamorphosed limestone), albeit intensely sheared and altered, and with variable local components of infill.

Coward (2001) argued that the HWSZ and FWSZ form part of a linked duplex of at least four faults or shear zones. The strike of this combined structure anastamoses between approximately NNE and ENE on a 10 km scale. The orebody is located at a pronounced flexure in the shear fabric associated with this structure. Coward (2001) demonstrated that in the vicinity of the mine, kinematic indicators suggest normal displacement on the shear zones, and that NNE-SSW directed

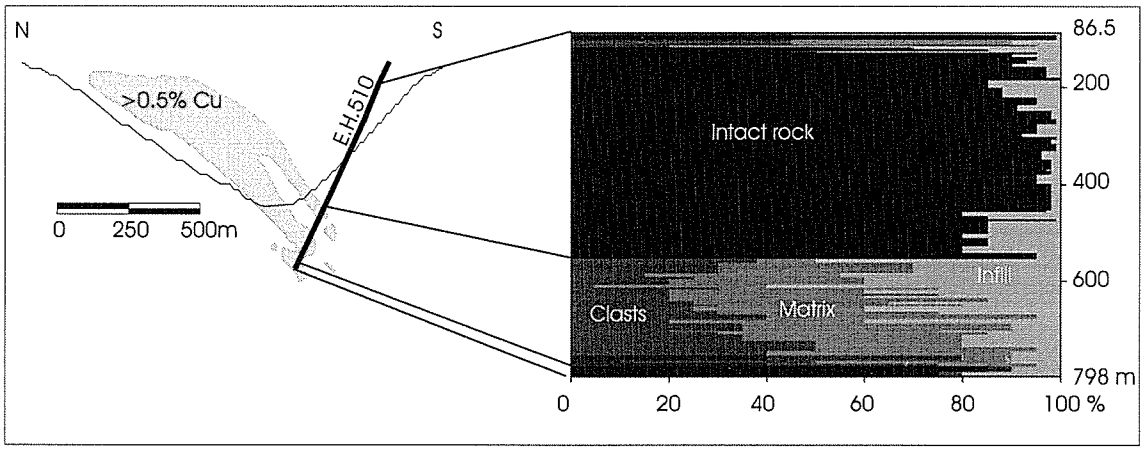

FIGURE 5.11.
Outline of the Ernest Henry deposit in cross-section, graphical log illustrates the relative proportion of intact rock, clasts, matrix and infill along diamond-drill hole EH510. The main ore breccia is predominantly matrix supported, with high components of both matrix and infill.

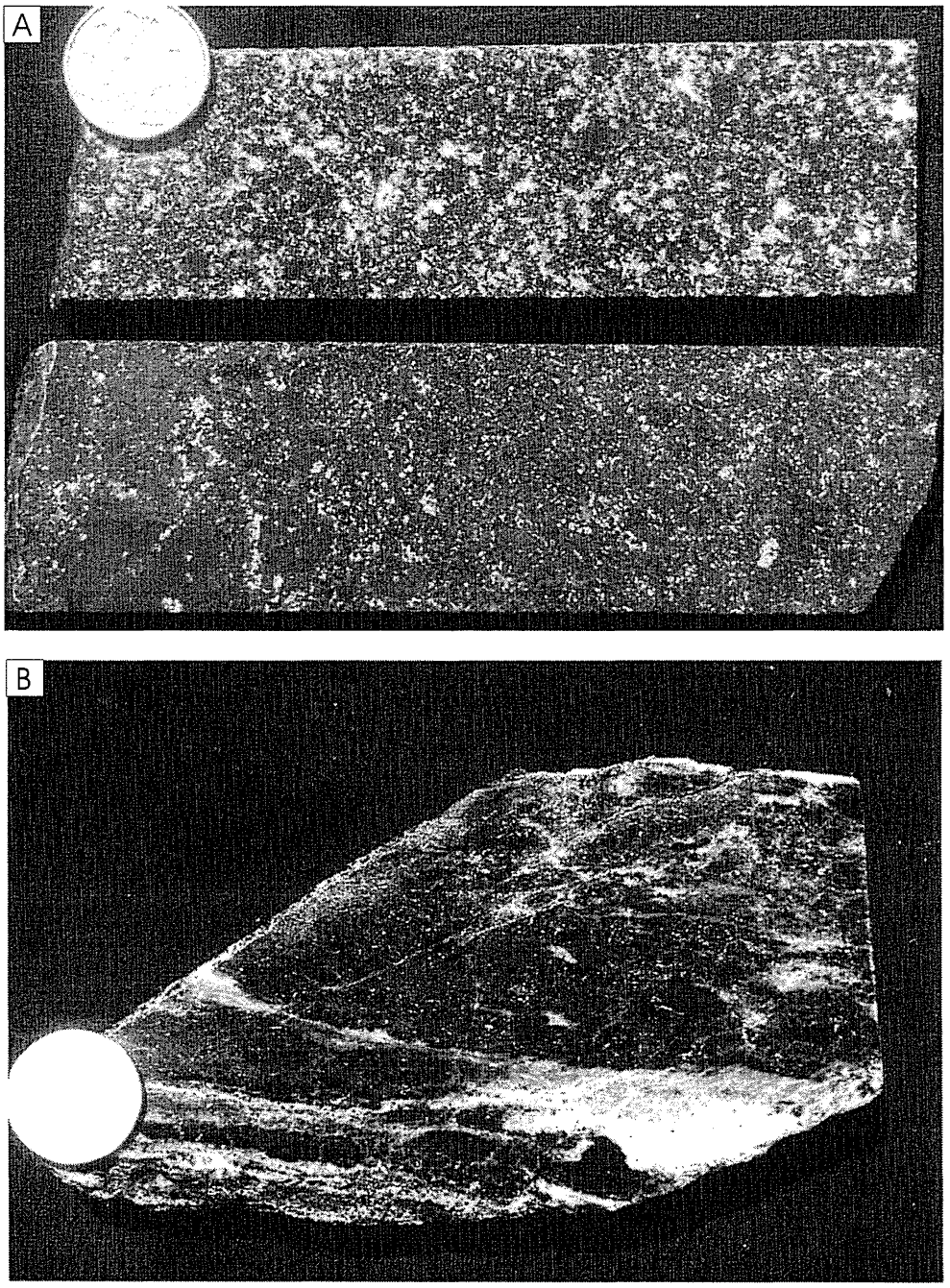

FIGURE 5.12.
(a) The monomict, milled ore breccia at Ernest Henry is variably infill- to matrix- supported (top and bottom respectively). Infill is largely represented by calcite (white). (b) Intensely sheared marble matrix breccia from the footwall to the Ernest Henry deposit. Diameter of coin in each photo = 2.4cm diameter.

shortening resulted in dilation localized at the flexure in the shear zones. Brecciation and mineralisation are similarly localized at this flexure.

Systematic logging of diamond drill hole EH510 was undertaken in order to quantify the ratios of breccia components along a representative section orthogonal to the orebody (Fig. 5.11). Where EH510 cuts the main orebody, the ore breccia has an apparent thickness of nearly 200m, characterized by a complete lack of intact wallrock, an average of 30 percent clasts, 43 percent comminuted matrix and 27 percent infill. The main ore breccia is predominantly matrix- and locally infill-supported (Fig. 5.12). Clasts are predominantly rounded, are derived from felsic volcanic rocks, and the matrix component to the breccia is the finely comminuted and metasomatised product of the same. An increase in the ratio of matrix and clasts to infill is noted towards the base of the breccia body.

Key characteristics include the location of the Ernest Henry deposit at a dilational flexure in a normal shear zone, and at the contact between predominantly ductile marbles in the footwall and more brittle, but locally sheared volcanics in the hangingwall. Also significant are the intense rounding of clasts, but lack of evidence for significant clast transport or mixing, and the matrix- and locally infill-supported nature of the ore breccia.

5.3 DISCUSSION

While each of the examples described above is located at a dilational fault jog or flexure, the resultant breccias and veins differ markedly in character (Fig. 5.13). Following, mechanisms that may explain the similarities and differences in breccia and vein style at the above localities are considered.

5.3.1 Clast generation and implosion brecciation

Breccia clasts in fault zones can be generated through a number of mechanisms. As emphasized by Sibson (1986) fault zones commonly initiate as interconnected meshes of shear- and extensional-fractures. As fault slip proceeds, cataclasis may further break the rock mass into isolated clasts. Alternatively, clast formation may occur by implosion brecciation (Sibson, 1986). Rapid fault slip

	Mount Elliott		Roxmere-Marimo		Tribulation Quarry		Gilded Rose	Ernest Henry
schematic geometry large width vein crackle breccia milled breccia dolerite	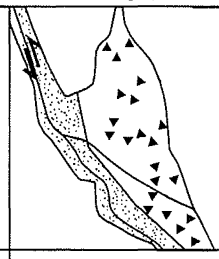		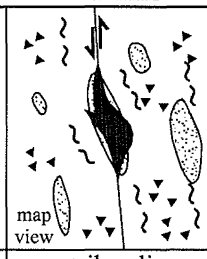		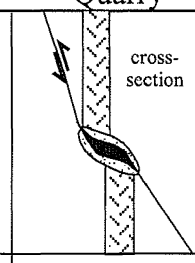		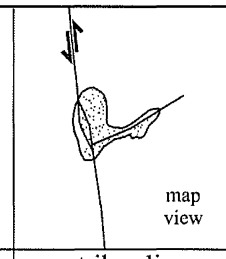	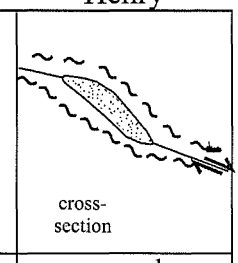
Fault mode	reverse		strike-slip		reverse		strike-slip	normal
Vertical continuity	~200 m		~50-100 m		~10 m		>1000 m	>500 m
Feature	milled breccia	crackle breccia	milled breccia	vein	milled	vein	milled breccia	milled breccia
Components	c>m>i	c>i>m	c>m>i	i>c	c>m>i	i	c~m>i	c~m~i
Clast shape	rounded	angular	rounded	angular	rounded	n.a.	rounded	rounded
Clast transport	1-20m	<2m	1-20m	<2m	1-20m	n.a.	10m to >1km	<100m
Inferred mechanism of brecciation or veining	implosion brecciation fuidization cataclasis	***implosion brecciation***	implosion brecciation fluidization cataclasis	implosion brecciation ***large width veining***	implosion brecciation fluidization cataclasis	***large width veining***	magmatic-hydrothermal explosion implosion brecciation ***gas streaming***	magmatic-hydrothermal explosion implosion brecciation ***fluidization***

FIGURE 5.13.
Summary diagram illustrating the key features of each of the examples presented. Vertical continuity is an estimate of the depth range over which increased permeability may have allowed for the attainment of near hydrostatic fluid pressure gradients (although not necessarily at hydrostatic fluid pressure values).
Components: clasts (c), matrix (m) and infill (i) are listed in order relative to their average abundance. The inferred dominant genetic mechanism is given in italics

commonly results in the generation of void spaces at dilational fault jogs, and where pressure differences between void spaces and the surrounding rocks exceeds the tensile strength of the rock, tensile failure results in implosion brecciation, or spalling of wallrock clasts into the void (Fig. 5.14a). Implosion breccias are characterized by high-dilation, angular clasts, little evidence for frictional attrition and exploded jigsaw textures (e.g. Phillips, 1972; Sibson, 1986). Vertically continuous dilational zones provide an additional setting for implosion brecciation. As a dilational zone fills with fluid, a hydrostatic fluid pressure gradient may be approached within the zone. Where the fluid pressure difference between the fault zone and the wallrocks exceeds the tensile strength of the rocks, implosion brecciation may continue even after the zone fills with fluid (Fig. 5.14b).

Application to field examples

Due to a large component of dilation at each of the areas described in this contribution, implosion brecciation should be considered a possible mechanism for the generation some clasts at each locality. Evidence for implosion brecciation is best preserved at Mt Elliott, whereas at the other localities subsequent clast transport has obscured the clast genesis mechanism, and clast genesis by interconnection of multiple fracture sets is also plausible. The outer carapace breccia at Mt Elliott is characterized by a large component of infill, sheeted tension gashes, large vugs, angular breccia clasts, clast-supported textures, a lack of significantly transported clasts, and void spaces that are now largely filled with coarse-grained hydrothermal precipitates, including significant sulphide minerals. These features are consistent with formation by means of implosion brecciation (e.g. Sibson, 1986). At Gilded Rose, the size of the breccia body relative to the inferred size of the dilational jog at which the breccia is localized may also reflect incorporation of wallrocks into the breccia by means of implosion brecciation.

Implosion brecciation is driven by the pressure difference between dilational zones and their immediate wallrocks (Sibson, 1986). This gradient is in turn a function of the rate at which dilational zones open, and the rate at which they fill

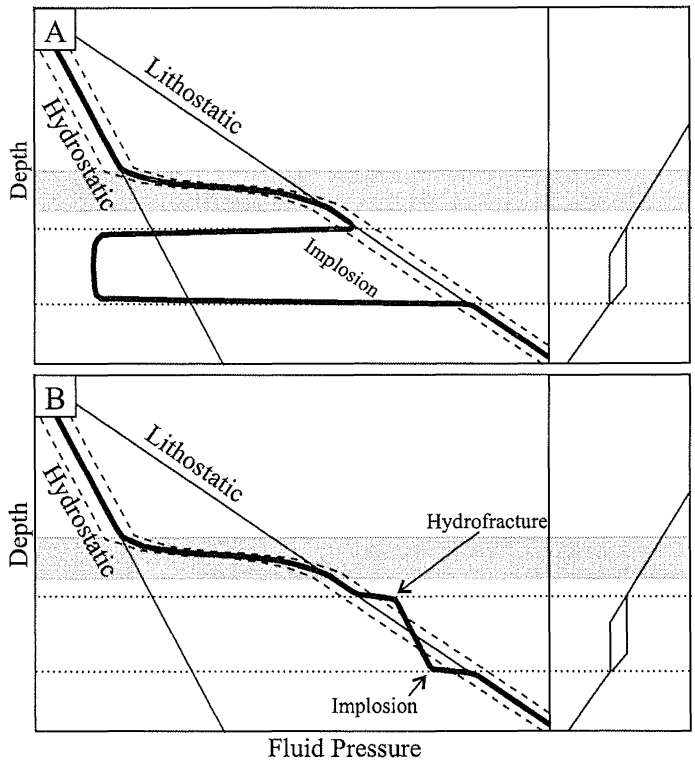

FIGURE 5.14.
Schematic fluid pressure curves for implosion brecciation. (a) Immediately upon fault-slip, fluid pressure within a dilational zone (bold, solid curve) may have a very low, and possibly near-zero fluid pressure value. The fluid pressure gradient between the dilational zone and the immediate wallrocks may exceed the extensional failure criteria (dashed curves), resulting in implosion brecciation. (b) As a dilational zone fills with fluid, a near hydrostatic gradient may be established. For vertically continuous zones, the pressure difference between the dilational zone may exceed the extensional failure criteria, allowing for continued implosion brecciation at the base of the zone, and hydrofracturing at the top of the zone.

with fluid. Thus, large magnitude and rapid tectonic slip, and low-permeability wallrocks will promote implosion brecciation.

5.3.2 Large width veining

The Tribulation and Marimo veins resemble extensional veins, characterized by large vein widths and locally preserved exceptionally coarse grain sizes. Vein textures record essentially continuous mineral growth, indicating that the rate of crack opening was greater than the rate of mineral infilling. In order to form extensional cracks in compressional environments, differential stress levels must remain low (σ_1-σ_3<4T, where T is the tensional strength of the rock), and fluid pressure must exceed least compressive stress by the tensile strength of the rock (P_f=σ_3+T) (e.g., Secor, 1965; Etheridge, 1983). This is a common phenomenon in metamorphic rocks, and extensional veins have been documented to depths of as much as 30 km (Ague, 1995). Void spaces that open rapidly are potentially subject to implosion brecciation as described above, however, this process cannot explain the genesis of the Tribulation vein, which is devoid of clasts.

Alternatively, an initially small fracture may propagate and widen, without implosion brecciation, if fluid pressure within the crack remains elevated during fracture propagation (i.e. fluid driven, hydraulic extensional fracturing; Fig. 5.15). For extensional fractures, fracture propagation is dependent on stress intensity, K_I, exceeding the fracture toughness (K_{IC}). Unlike tensile strength, fracture toughness is a failure criterion based on the heterogeneous stress field at a fracture tip (e.g., Pollard and Aydin, 1988). Stress intensity is given by:

$$K_I = (p - \sigma_3^r)(\pi a)^{1/2}$$

where 'p' is the fluid pressure within the fracture, 'σ_3^r' is a uniform remote stress, and 'a' is half of the length of the fracture (Pollard and Aydin, 1988). Fracture propagation will be favored in areas of reduced σ_3 and for initially longer fractures. Thus in highly fractured rocks or breccias, fracture propagation may be preferentially localized in a single fracture, or a small number of initially longer fractures, and early brecciation may give way to propagation of these fractures.

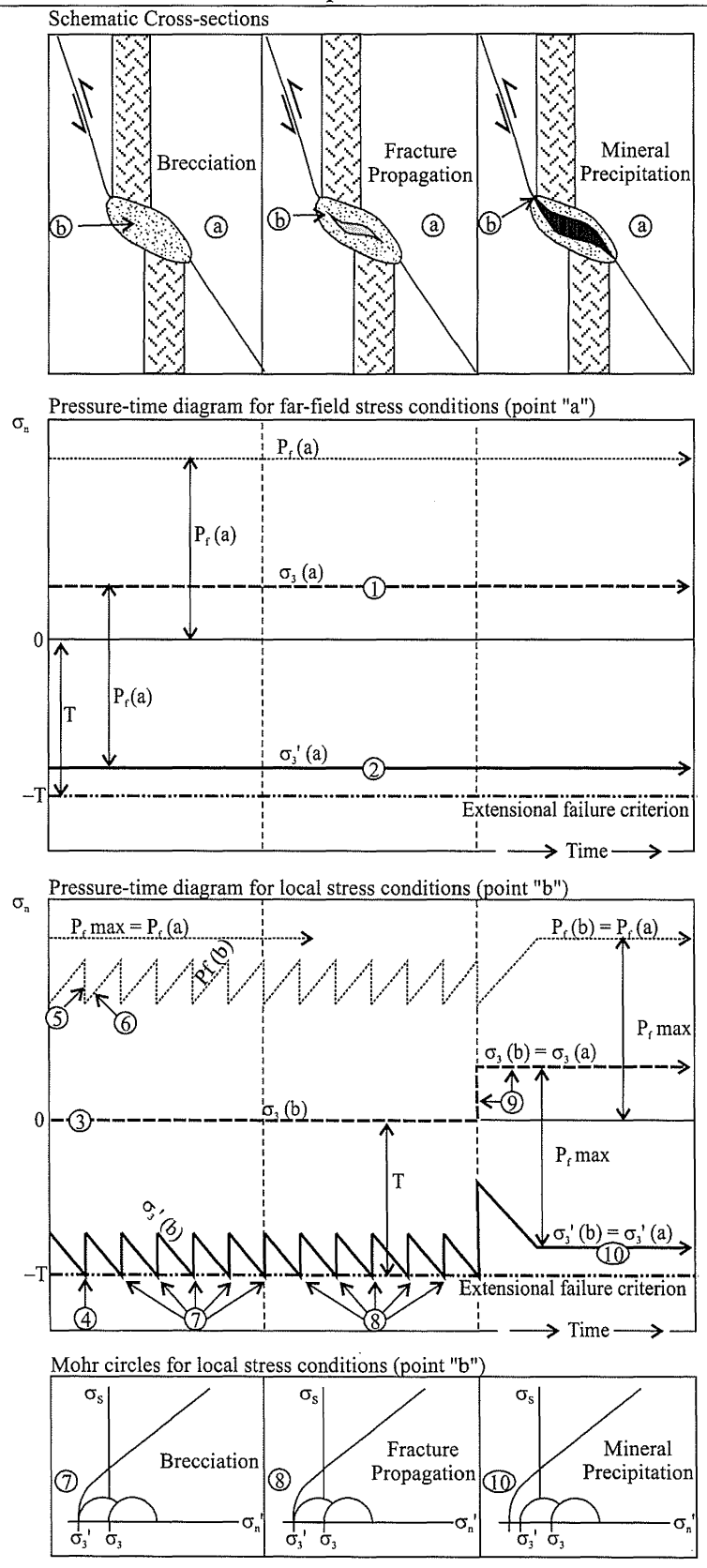

FIGURE 5.15.
See following page.

FIGURE 5.15.
Model including schematic cross-sections, pressure-time diagrams and Mohr circles for the genesis of large width veins, at for example, Tribulation. Point "a" in the cross-sections represents far-field stress conditions, whereas "b" represents local stress conditions, as indicated. The stippled region represents an area of reduced σ_3, reflecting a stress shadow at the dilational intersection between a fault and a competent dolerite body. Numbered points on the pressure-time diagrams and corresponding Mohr circles correspond with the descriptions given below.

The pressure-time diagram for far-field stress conditions reflects:
1) σ_3 (a) remains constant with time.
2) Fluid pressure, Pf (a), is insufficient to cause σ_3' (a) to meet the extensional failure criterion and extensional failure does not occur. The pressure time diagram for local stress conditions reflects:
3) σ_3 (b) is reduced relative to the far-field stress conditions (i.e. σ_3 (b) < σ_3 (a)), and in this example has been given a value of zero. Weakly negative values of σ_3 (b) are also plausible.
4) An increase in fluid pressure, P_f(b), driven by higher fluid pressure in the surrounding rocks, causes σ_3' to meet the extensional failure criterion, resulting in extensional failure.
5) Upon extensional failure, fluid pressure drops in the vicinity of the newly formed fracture.
6) Because P_f (b) is less than P_f (a) fluid will flow towards point "b", allowing for recharge of fluid pressure in the vicinity of the initial fracture.
7) Repeated extensional failure results in brecciation.
8) Fracture mechanics dictates that with repeated extensional failure, continued failure may become concentrated at the tips of a single larger fracture, and as such the initial brecciation stage may give way to a fracture propagation stage.
9) As the fracture propagates outside of the zone of reduced σ_3, stress conditions at the crack type will reflect the far-field stress conditions (i.e. σ_3 (a) = σ_3 (b)).
10) Because of the increased value of σ_3 (b) at the crack tip, the failure criterion will no longer be met, stopping fracture propagation. However, so long as σ_3' (b) is negative, the fracture will be held open, allowing for mineral precipitation into the fracture.

Fracture arrest occurs either as a result of a decrease in fluid pressure within a fracture, an increase in the remote compressive stress (σ_3^r), or an increase in fracture toughness. Decreased fluid pressure results from the increased volume of a growing fracture (Secor, 1969; Pollard and Aydin, 1988) and the general low permeability of metamorphic rocks imposes a limit on the rate at which fluid can be recharged. In contrast, in high permeability rocks, including breccia zones, fluid within propagating fractures may be more readily recharged, thereby limiting the extent to which fluid pressure fluctuations can affect fracture propagation. Alternatively, fractures initiated in zones of reduced σ_3^r and/or reduced tensile strength of the rock may be arrested as they propagate outside of these zones.

From the above arguments, we propose that the genesis of large width veins including the Tribulation and Marimo veins, was facilitated by reduced least principal compressive stress, significant fluid overpressuring and the highly permeable nature of the breccia bodies that host the veins.

Deformation subsequent to mineral precipitation in large width veins in the Eastern Succession appears to have been predominantly accommodated by shearing in the relatively weak calcite-dominated veins, as opposed to ongoing brecciation. In relatively rare cases such as at Tribulation where coarse grain sizes are completely preserved in the veins, subsequent deformation may have been accommodated by adjacent structures.

5.3.3 Clast transport, fluidization and gas streaming

There are a limited number of mechanisms by which breccia clasts may be transported. In near surface and karst environments, gravitational collapse can result in downward clast transport. Collapse breccias are characterized by blocky and angular clasts with negligible rounding, limited mixing, a minor or absent matrix component and commonly large infill spaces (Taylor and Pollard, 1993).

Slip along fault zones can lead to attrition brecciation, and clast transport within the plane of the fault (Sibson, 1986). The magnitude of clast transport by this mechanism, however, cannot exceed the magnitude of fault slip, imposing a significant limit on clast transport distance. Attrition breccias are characterized by a

limited degree of clast mixing, clast rounding, a large matrix component, a near absence of infill, locally strong matrix fabrics and internal clast deformation (e.g. Sibson, 1986; Taylor and Pollard, 1993).

Magmatic-hydrothermal breccias are forced, largely upwards, in response to large pressure gradients, typically the result of magma emplacement at depth (e.g. Sillitoe, 1985). The breccias exhibit a large degree of clast rounding, a variable matrix component, a small infill component and small to moderate degrees of clast transport and clast mixing (e.g. Taylor and Pollard, 1993). Where the force driving clast transport is propagated predominantly across contacts between adjacent clasts (as opposed to clasts being entrained in a fluid or gas flow, see below), and the breccia mass is squeezed along cracks as a wet slurry from areas of high to lower pressure, the resultant breccias are referred to here as forced magmatic-hydrothermal breccias. This provides a potential, albeit likely inefficient, mechanism for clast transport.

Alternatively, clasts in magmatic-hydrothermal breccias may be transported by rapidly moving fluids and gasses, either by magmatic-hydrothermal explosion involving rapid fluid volume expansion (e.g. Laznicka, 1988), or by fluidization and gas-streaming processes. Fluidization refers to an industrial process, and the term was first applied to geological processes by Reynolds (1954). Wohletz and Sheridan (1979) define a fluidized system as "a mixture of particles (solid or liquid) suspended in an upward escaping fluid phase (liquid or gas) so that the frictional force between the fluid and the particles counterbalances the weight of the particles and the whole mass behaves as a fluid." With increasing fluid velocity, particles may be significantly transported upwards, in a process commonly referred to as gas streaming (e.g. Wolfe, 1980; McCallum, 1985). Employing the above definitions, breccias which contain clasts that were transported in a rapidly moving fluid can be referred to as explosive breccias where the fluid or gas movement was short-lived, or gas stream breccias, where rapid fluid or gas flow was sustained over a period of time. Usage of the term fluidized breccia should be limited to instances where breccia clasts were suspended (but not significantly transported upwards) in a fluid or gas flow. Explosive, gas stream and fluidized breccias commonly contain a large

matrix component and varying degrees of clast mixing, rounding and transport (up and/or down; Laznicka, 1988; Taylor and Pollard, 1993)). Transport mechanisms may be difficult to distinguish from one another, although explosive breccias may contain a greater range in clast size, relative to fluidized or gas stream breccias (e.g. Wolfe, 1980). By their nature, explosive, fluidized and gas stream breccias are prone to gravitational collapse prior to cementation, and as such, direct evidence of clasts having been suspended or transported by a fluid or gas may be poorly preserved. For example, Taylor and Pollard (1993) note that voids or infill within these breccias are typically uncommon and small, presumably reflecting gravitational collapse and settling of breccia clasts prior to cementation.

Infill-supported breccias can be produced by superposition of multiple veining episodes, gravitational collapse, explosion, fluidization or gas streaming. Given that clasts in collapse breccias are typically angular and show little clast mixing (Taylor and Pollard, 1993), the occurrence of polymict, infill-supported breccias with well-rounded clasts, and which lack evidence for multiple fracture episodes, may record explosion, fluidization or gas-streaming. Such an interpretation is particularly applicable where upward clast transport is recorded.

Application to field examples

Mt Elliott, Tribulation, the Roxmere-Marimo, the Gilded Rose type area and the HWSZ at the Ernest Henry deposit each contain paragenetically early milled breccias. A large matrix and small infill component, minor to moderate clast transport, and locally developed matrix fabric and clast deformation characterize the breccias. These breccias are interpreted as a combination of attrition breccias and forced magmatic-hydrothermal breccias. A component of explosion, fluidization, or gas-streaming is also possible in response to moderate fluid pressure fluctuations associated with faulting, but unequivocal evidence for these processes has not been documented in these early breccias.

In the Gilded Rose breccias, the variable but predominantly rounded nature of clasts, evidence for significant upwards clast transport, a high component of rock-flour matrix and locally a high component of infill are consistent with clast

transport via explosion or gas streaming (e.g. McCallum, 1985; Taylor and Pollard, 1993). The ore breccia at Ernest Henry is a milled, matrix- and infill-rich breccia that is locally infill-supported, and may record similar processes. A lack of significant clast mixing or evidence for significant clast transport in the Ernest Henry ore breccia may record fluidization. However, it is also possible that infill supported ore breccias at Ernest Henry resulted from superposed fracturing events, evidence for which has been obscured by subsequent shearing, now poorly recorded in the carbonate rich ore assemblage.

Factors promoting fluidization and gas streaming

As discussed above for implosion brecciation, when a highly permeable dilational zone fills with fluid, a hydrostatic fluid pressure gradient (although not necessarily at hydrostatic fluid pressure values) will be approached within the zone of fluid connectivity (Fig 5.2). Where emplaced in rocks at suprahydrostatic or lithostatic pressure, the base of dilational zones within faults will be underpressured with respect to the surrounding rocks. In addition to implosion brecciation, this will result in fluid flow into the base of the zone of dilation, and out of the top of the zone of dilation, forcing a deviation in the fluid pressure gradient away from hydrostatic (Fig. 5.16a). This deviation will result in fluid flow up along the dilational zone. Where fluid flux is sufficiently large, this process has the potential to result in fluidization or gas streaming within the fault.

The magnitude of the deviation of the fluid pressure gradient along the fault zone away from hydrostatic depends on the rate of fluid flux into the base of the zone of dilation and out of the top of the zone of dilation. This rate is governed largely by the fluid pressure gradient between the fault and its wallrocks, and the wallrock permeability.

For dilational faults emplaced in rocks at near lithostatic fluid pressures, the magnitude of pressure differences between the faults and their surrounds, and consequently the potential for fluidization and gas streaming is a function of the vertical continuity of the dilational zone (Fig. 5.2). This is in turn a function of the orientation of the fault, the magnitude of fault slip, and the size of the dilational jog

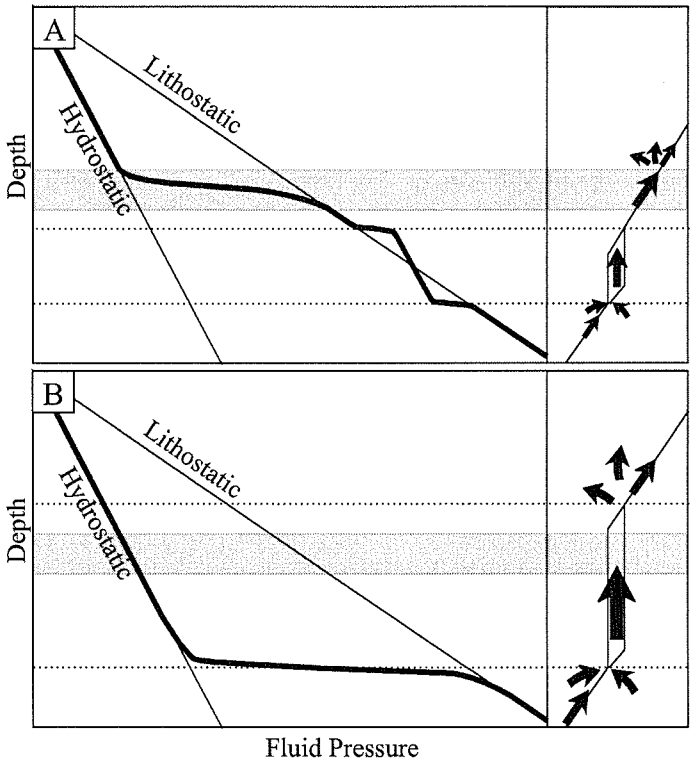

FIGURE 5.16.
Schematic fluid pressure curves for fluidization and gas streaming, shown here for normal faults. After fault slip, fluid pressure (dashed curve) within dilational zones will strive to attain a hydrostatic gradient, although not necessarily at hydrostatic values. (a) Where emplaced within rocks at near-lithostatic pore fluid pressure, this will result in underpressuring at the base of the dilational fault segment, and overpressuring at the top of the zone. This will result in fluid flow into the base, and out of the top of the dilational zone, resulting in net upward fluid flow. (b) Where a dilational zone straddles the transition between near-lithostatic fluid pressure at depth, and near-hydrostatic fluid pressure in the shallow crust, fluid pressure may drop to near-hydrostatic values along the depth of the dilational zone, resulting in extreme underpressuring at the base.

(Fig. 5.2). Steep faults, large fault slips, and large dilational jogs will all favor greater dilational zone vertical continuity. A further and more critical control is found in the fault mode. While dilational jogs in reverse, strike-slip and normal faults will result in dilational zones of similar shape, the long axis of these zones will be horizontal for normal and reverse faults, and vertical for strike-slip faults (Fig. 5.2; Cox et al., 2001; Sibson, 2001). Consequently, dilational zones in strike-slip faults may have very large vertical continuity, even with minor fault slip. Thus, assuming vertical fluid pressure gradients are on average greater than horizontal gradients, fluidization and gas streaming are more likely to occur in strike-slip faults. The intermediate axis of dilational zones will be a function of either the length of the fault jog, or the magnitude of displacement, which ever is greater. For example, in Figure 5.2b schematic fault jogs are shown with relatively long fault jogs and small displacement, and in these cases, the intermediate axis of the dilational zones is equal to the length of the dilatant jog. For normal faults, dilational zones of considerable vertical continuity can be established with relatively minor fault slip if dilational jogs are significantly large. For reverse faults, vertically continuous dilational zones require large magnitude fault slip. Thus, normal faults may be more prone to fluidization and gas steaming than are reverse faults.

The situation in which a dilational fault zone straddles the transition between rocks at near lithostatic fluid pressure at depth to near hydrostatic in the shallow crust, may result in fluid pressure drops to near hydrostatic values (and gradients) to the base of the dilational zone (Fig. 5.16b). This will result in even more extreme fluid pressure gradients than for dilational zones emplaced entirely within rocks at suprahydrostatic values. Diatreme behavior whereby breccia pipes reach the surface may result.

In addition to large fluid pressure gradients, fluidization and gas streaming require very large fluid fluxes. This in turn requires a substantial fluid source or sources. With respect to the Gilded Rose breccias, it has been noted that all occurrences of these breccias are underlain by Corella Formation rocks and Corella breccias. The Corella breccias are characterized by brecciated meta-siltstone and calc-silicate rock sequences separated by low-permeability ductile marble horizons

(**Chapter 4**, this study), and may have acted as a series of stacked fault-fracture meshes (Hill, 1977; Sibson and Scott, 1998). Overpressured fluids within the Corella Breccias may have triggered reactivation of existing faults, linking of originally isolated fluid compartments, and catastrophic discharge of fluid out of large volumes of rock upon fault slip.

Additionally, some fluid may have been directly sourced from granitoids. The Gilded Rose breccias commonly contain intrusions with miarolitic cavities, spherulites and porphyritic textures. Miarolitic cavities are taken as evidence for volatile saturation prior to complete melt crystallization (London, 1992; Candela and Blevin, 1995). Spherulites and porphyritic textures are believed to be the result of undercooling in crystallizing magmas (Fenn, 1977; Swanson and Fenn, 1986; Candela, 1997). Undercooling may result from either a rise in the liquidus temperature of a magma in response to a release of fluids from the melt (Candela, 1997; Perring *et al.*, 2000), or rapid ascent and cooling of the melt. These textures may indicate that granitoids within the Gilded Rose breccias were partly molten at the time of brecciation. Large pressure drops and/or the rapid ascent of magmas within fault zones may have induced rapid fluid exsolution.

Large fluid pressure drops associated with faulting may have promoted fluid unmixing in H_2O-CO_2-NaCl fluids (Bowers and Helgeson, 1983; Burnham, 1985; Pollard, 2001), either directly exsolved from crystallizing intrusions, or drawn out of the Corella breccias as discussed above. Volume expansion associated with unmixing (i.e. magmatic-hydrothermal explosive behavior; Laznicka, 1988), may have further driven upward flow of fluids and entrained breccia clasts.

5.3.4 Catastrophic fault valving

In contrast to many examples of dilational jog related fault breccias in which evidence for multiple superimposed slip and associated brecciation events are recorded, some of the breccia occurrences presented here appear to be associated with a single slip event. This is particularly noted at the Gilded Rose type area, where a single catastrophic fluid flux episode is inferred to have resulted in explosive gas expansion and/or gas streaming of breccia clasts. In the case where

existing faults are optimally oriented for reactivation (i.e. at approximately 30° to σ_1), fault reactivation can occur at relatively low levels of fluid overpressuring. Repeated small-magnitude slip events and episodic release of overpressured fluids would be the likely result. Catastrophic fault valve action is more likely where early-formed through-going faults are not present, or where existing through-going faults are severely misoriented for reactivation (ie. at >50-60° to σ_1), and slip on these structures is in response to severe fluid overpressuring (Sibson, 2001 and references therein). At the Gilded Rose type area, the controlling fault appears to have been optimally oriented for D_3 slip. As such, inferred catastrophic fault valving may record initial development of the fault zone. Subsequent fault reactivation would have occur at lower levels of fluid overpressure, and as such would not be expected to have triggered catastrophic fault valve behavior.

5.4 CONCLUSIONS

In the examples of breccias and veins described above, milled attrition breccias and forced magmatic hydrothermal breccias are common, regardless of fault mode. Implosion brecciation is also likely common in all fault modes, but evidence is only well preserved where clasts have not been subsequently transported through other processes. In the Eastern Succession, both steep and shallow-dipping large width veins (>1m width) are documented within structures of different fault mode, suggesting that fault mode and orientation are of secondary importance in the genesis of these veins. It is proposed that large width veining is dependent on expansion of originally small fractures, and is favored by zones of locally decreased σ_3 and increased permeability. In contrast, extensional veins in low-permeability pristine metamorphic rocks tend to be small.

Fluidization and gas streaming require large fluid pressure gradients to drive rapid fluid flow. Such gradients can be established where the base of vertically continuous dilational zones are emplaced in near lithostatic-pressured rocks, and particularly where dilational zones bridge the boundary between lithostatic- and hydrostatic-fluid pressures. Fluidization and gas streaming are favored in strike-slip faults, and to a lesser degree in normal faults, as opposed to reverse faults. Large

magnitude fault slip, steep faults as well as large and steeply oriented dilational jogs and extreme fault valve action on severely misoriented faults all favor these processes. Fluidization and gas streaming are also dependent on large fluid volumes that can rapidly flow into dilational zones. Highly permeable rocks, such as tectonic breccias or meshes of interconnected fractures, may be required near the base of fault zones as a precursor to fluidization. Fluid exsolution from granitoids in response to pressure drops can provide an additional fluid source.

While the examples referred to in this contribution all exhibit features developed during the waning phases of the Isan Orogeny in the Eastern Fold Belt, differences in fault mode (i.e. strike-slip, reverse or normal) in part explain the nature of the resultant breccias and veins. These differences in fault mode can be related to a regional shift from compression to transtension during this period (O'Dea et al., 1997), as well as to local variations in the orientation and magnitude of the principal applied stresses in a heterogeneous and increasingly brittle terrane. As noted by Sibson and Scott (1998), and Sibson (2001), the containment of overpressured fluids is less frequent in extensional and to a lesser degree in strike-slip environments than in compressional environments. Of the examples presented, inferred fluidization and gas streaming processes at the Ernest Henry and Gilded Rose locales require the greatest fluid fluxes. These examples are associated with extensional and strike-slip settings respectively. Significantly, Ernest Henry contains the largest Cu-Au resource in the Eastern Succession. This gives credence to the importance of a shift from compression to wrenching, and in the case of Ernest Henry, local extension, in focussing large volumes of metasomatic fluids into discrete structural conduits, a process critical in the genesis of large epigenetic ore deposits. Such a shift may be manifest throughout a district, or only recorded locally as a result of heterogeneity in the regional stress field.